

The contribution of mitochondria-associated ER membranes to cholesterol homeostasis

¹Montesinos, J.*#, ²Kabra K.*, ¹Uceda, M., ³Larrea, D., ²Agrawal, R.R., ²Tamucci, K.A., ³Pera, M., ¹Ferre, A.C., ¹Gomez-Lopez, N., ¹Yun T.D., ³Velasco K.R., ^{3,4}Schon E.A., and ^{1,3}Area-Gomez, E.#

1. Centro de Investigaciones Biológicas Margarita Salas. CSIC. Madrid, Spain. CIBERNED.
2. Institute of Human Nutrition, Columbia University Irving Medical Center, New York, NY, USA.
3. Department of Neurology, Columbia University Irving Medical Center, New York, NY, USA.
4. Department of Genetics and Development, Columbia University Irving Medical Center, New York, NY, USA.

Keywords: Mitochondria-associated membranes (MAM), cholesterol, HDL, ACAT1, SR-B1, squalene monooxygenase.

*These authors contributed equally to this work

#Corresponding authors: estela.area@cib.csic.es; jorge.montesinos@cib.csic.es.

ABSTRACT

Cellular demands for cholesterol are met by a balance between its biosynthesis in the endoplasmic reticulum (ER) and its uptake from lipoproteins. Cholesterol levels in intracellular membranes form a gradient maintained by a complex network of mechanisms including the control of the expression, compartmentalization and allosteric modulation of the enzymes that balance endogenous and exogenous sources of cholesterol. Low-density lipoproteins (LDLs) are internalized and delivered to lysosomal compartments to release their cholesterol content, which is then distributed within cellular membranes. High-density lipoproteins (HDLs), on the other hand, can transfer their cholesterol content directly into cellular membranes through the action of receptors such as the scavenger receptor B type 1 (SR-B1; gene *SCARB1*). We show here that SR-B1-mediated exogenous cholesterol internalization from HDL stimulates the formation of lipid-raft subdomains in the ER known as mitochondria-associated ER membranes (MAM), that, in turn, suppress *de novo* cholesterol biosynthesis machinery. We propose that MAM is a regulatory hub for cholesterol homeostasis that offers a novel dimension for understanding the intracellular regulation of this important lipid.

INTRODUCTION

Cellular membranes are highly dynamic entities involved in almost all cellular functions. The establishment and maintenance of the unique lipid composition of membranes are pivotal for cellular physiology (1). Each cell type has a characteristic lipidome established during development and tightly regulated thereafter by several intracellular and extracellular mechanisms. The relative levels of cholesterol are meticulously maintained, specially within different cellular membranes, where there is a gradient between the plasma membrane (PM), where most of the cell's cholesterol resides, and the endoplasmic reticulum (ER), which contains low levels of this lipid while also harboring the cell's cholesterol biosynthetic machinery (2). This tight regulation of cholesterol levels among cellular compartments is due in part to cholesterol's ability to alter membrane biophysical properties by promoting rigidity and, above a certain threshold, causing membrane partitioning and the formation of lipid raft (LR) domains (3, 4). These dynamic and rigid membrane LR domains segregate subsets of lipid-binding proteins and facilitate conformational changes and/or protein interactions to regulate specific pathways (5).

Cellular cholesterol levels are regulated, in part, by precisely balancing *de novo* synthesis in the endoplasmic reticulum (ER) and its internalization from extracellular lipoproteins through receptor-mediated mechanisms (2). Most cell types rely on the latter to fulfill their cholesterol needs, adjusting cholesterol biosynthetic activity through communication between the PM and the ER (6).

In mammalian cells, extracellular cholesterol is primarily internalized from the uptake of low-density lipoproteins (LDL). Briefly, after binding to low-density lipoproteins receptors (e.g., LDLR), LDL particles are endocytosed and fuse with lysosomes, triggering the hydrolysis of their constituent cholesterol esters (CE) into free cholesterol (FC) (7). FC is inserted into the endolysosomal membrane by the Niemann-Pick C (NPC) proteins 1 and 2 (NPC1 and NPC2). Evidence suggests that these cholesterol-rich endosomes first fill cholesterol PM pools up to a threshold, past which the excess cholesterol induces membrane invagination and the formation of cholesterol-rich endosomes that are transported to the ER (8-10).

To a lesser degree, mammalian cells can also acquire cholesterol from the extracellular medium by the internalization of high-density lipoproteins (HDL). This type of particle was previously considered to be mainly involved in cholesterol efflux (11). However, multiple lines of evidence indicate that cells can internalize cholesterol from these particles through HDL-avid receptors, such as the scavenger receptor B1 (SR-B1), to provide cells with extra cholesterol under specific conditions like steroidogenesis or LDL-deficiencies (12). Contrary to LDL, cholesterol from HDL particles is channeled directly towards cell membranes in a concentration gradient manner, rather than through the uptake of the holoparticle itself

(12). Moreover, while LDL-derived cholesterol moves first to the PM before the ER, HDL-cholesterol has been shown to be able to be delivered directly to the ER (13-15).

In the ER, increases in cholesterol levels delivered from the PM results in the formation of cholesterol-rich regulatory domains, capable of repressing cholesterol biosynthesis at the transcriptional and post-transcriptional levels. This maintains cholesterol homeostasis through the modulation of master lipid regulators such as the sterol regulatory element binding protein (SREBPs) (9, 16-21). Similarly, several reports have identified an intracellular cholesterol pool in membranes juxtaposed to the ER - also called the endocytic recycling compartment - that can sense cholesterol changes in the PM and induce feedback responses to maintain cholesterol levels (22, 23). However, the identity, localization, and regulation of these pools of cholesterol in the ER are not completely understood.

Mitochondria-associated ER membranes, or MAM, are transient lipid-raft domains in the ER in close apposition to mitochondria, involved in the regulation of lipid and calcium metabolism, as well as cellular bioenergetics (24, 25). Previous data from our lab have revealed an association between cholesterol internalization and delivery to the ER and the activation of MAM domains (26, 27). Here, we show that the formation of MAM is a consequence of the mobilization of excess cholesterol from the PM, resulting in the spatial clustering and repression of cholesterol biosynthetic enzymes. Moreover, we demonstrate that cholesterol internalization and MAM formation are specifically stimulated by cholesterol uptake from HDLs. Taken together, our data suggest that the formation of MAM is a key step in the regulation of cholesterol metabolism, fitting the description of previously described regulatory intracellular cholesterol pools, and provides a new framework for understanding how extracellular lipids modulate intracellular metabolic feedback responses.

RESULTS

Cholesterol internalization and its delivery to the ER induces the formation of MAM domains.

Our previous work indicated that, as a lipid-raft-like domain, the formation of MAM is triggered by elevated cholesterol levels in the ER (27). Interestingly, this increase was associated with the delivery of excess cholesterol to the ER from the PM, rather than with an increase in its *de novo* cholesterol biosynthesis. To confirm these data, we quantified the MAM activity after stimulating cholesterol uptake and traffic from the PM to the ER by incubating cultured cells with increasing concentrations of exogenously added cholesterol, as shown before (28). Specifically, we incubated human neuroblastoma cells (SH-SY5Y) (**Fig. 1A-B**) and mouse embryonic fibroblasts, MEFs (**Fig. S1A-B**) in medium containing 3% serum supplemented with increasing concentrations of water-soluble cholesterol (0.5 mg, 3 mg, or 5 mg per 100 ml), spiked with ³H-cholesterol, and measured its internalization and esterification over time. Under these conditions, cultured cells displayed a dose-dependent increase in

cholesterol uptake (**Fig. 1A**) and its delivery to the ER, resulting in the stimulation of MAM functions, including the esterification of cholesterol by acyl-coenzyme A: cholesterol acyltransferase 1 (ACAT1, gene *SOAT1*) (**Fig. 1B**) and the synthesis and transfer of phosphatidylserine to mitochondria for its decarboxylation into phosphatidylethanolamine (**Fig. 1C and Fig. S1C-D**) (29).

We corroborated these results by stimulating PM-to-ER cholesterol trafficking by adding exogenous sphingomyelinase (SMase) to our cell cultures (16). As expected, this treatment induced the internalization of cholesterol, its delivery to the ER (**Fig. 1D and S1E**), and its subsequent esterification by ACAT1 in both SH-SY5Y cells (**Fig. 1E**) and mouse fibroblasts (**Fig. S1F**). This stimulation of cholesterol delivery to the ER resulted in the concomitant activation of MAM functions (**Fig. 1F and S1G**) and an increase in ER-mitochondria apposition or contacts (MERCs) (**Fig. S1H**), while the inhibition of endogenous SMase by GW4869 (27) resulted in the opposite phenotype (**Fig. 1F**). In agreement, impairing cholesterol transport by incubation with (U18666A), an inhibitor of the NPC1 and of Aster-mediated cholesterol trafficking (30), impeded the activation of MAM even after SMase treatment (**Fig. S1I**). Conversely, inhibition of 3-hydroxy-3-methyl-glutaryl-CoA reductase (HMGCR), the first rate-limiting enzyme in the mevalonate pathway, did not significantly impact MAM activities (**Fig. S1J**), confirming that the observed phenotypes were not attributable to *de novo* cholesterol synthesis.

Our data thus indicate that cholesterol mobilization from the PM induces transient increases in cholesterol in the ER and induces the formation and activation of MAM domains.

The formation of MAM represses cholesterol biosynthesis.

Cholesterol delivery to the ER represses cholesterol biosynthesis by allosterically inhibiting the activity of specific rate-limiting enzymes and repressing SREBP2 (gene *SREBF2*) processing and expression. In agreement, our data show that SMase treatment and subsequent MAM activation resulted in a decrease in the protein levels of both the precursor and mature forms of the cholesterol biosynthesis master regulator, SREBP2 (**Fig. S2A**), and subsequently reduced the expression and activity of the rate-limiting cholesterol biosynthetic enzyme HMGCR (**Fig. 2A**). Interestingly, SMase treatment did not affect the transcription levels of several of its downstream enzymes, such as squalene synthase (SQS; also called farnesyl-diphosphate farnesyl transferase, gene *FDFT1*), squalene monooxygenase epoxidase (SQLE; *SQLE*), or the lanosterol synthase (LSS) (**Fig. S2B**).

To study the relationship between cholesterol biosynthesis and MAM, we examined the protein composition of MAM fractions using a PhotoClick-cholesterol proteomics approach (31), as before (27). Briefly, cultured cells were incubated with the PhotoClick-cholesterol probe, MAM fractions were isolated, the probe crosslinked to cholesterol-interacting proteins and conjugated to the probe's azide-

biotin tag by click chemistry. These cholesterol-interacting tagged proteins were pulled down using streptavidin beads and identified by mass spectrometry.

Our results indicated that various enzymes from the *de novo* cholesterol synthesis and cholesterol turnover pathways were present in MAM domains (**Fig. 2B**), and interacted with cholesterol, as shown before (32). While levels of HMGCR were detectable at MAM, the post-squalene branch of cholesterol biosynthesis was particularly enriched (33), including the rate-limiting enzymes squalene synthase (SQS; FDFT1) and squalene monooxygenase epoxidase (SQLE; SQLE), along with other pathway components: lanosterol synthase (LSS), cytochrome P450-51A (CYP51A1), NAD-sterol dehydrogenase (NSDHL), 24-dehydrocholesterol reductase (DHCR24), and 7-dehydrocholesterol reductase (DHCR7) (32, 34, 35). Additionally, we found well-known MAM-resident enzymes, such as the ER lipid raft associated protein 2 (ERLIN2; *ERLN2*), which inhibits the *de novo* synthesis of cholesterol by inducing the degradation of HMGCR (36, 37), and ACAT1 (*SOAT1*), which mediates cholesterol esterification (38, 39).

To validate these data, we also examined the subcellular localization of these cholesterol biosynthesis enzymes using subcellular fractions from mouse brain (40). In agreement with our proteomics results, we found that within the ER, post-squalene synthesis enzymes were enriched at MAM (**Fig. 2C**).

Altogether, our data led us to conclude that the formation of MAM induces a feed-back response that inhibits cholesterol biosynthesis, perhaps via the spatial clustering and modulation of the post-squalene enzymatic machinery and/or ERLIN2 (41).

MAM formation induces cholesterol internalization and its delivery to the ER.

To further test the relevance of MAM regulation in the control of cholesterol metabolism, we measured cholesterol uptake and synthesis in cell models where MAM formation is either impaired or enhanced due to the ablation of mitofusin 2 (MFN2-KO cells) or presenilins-1 and -2 (PSEN1/2-KO; PS-DKO), respectively, as previously shown (42). MAM-deficient MFN2-KO cells showed reductions in the internalization of exogenous cholesterol from the PM and concomitant increases in cholesterol biosynthesis and HMGCR expression, while PS-DKO cell models, where MAM is constitutively upregulated, showed the inverse phenotype (**Fig. 3A-D and S2C**).

To stimulate cholesterol influx and its delivery to the ER, we exposed MAM-deficient cells to increasing concentrations of fetal bovine serum (FBS, containing cholesterol) or exogenous cholesterol in the medium. Compared to controls and PS-DKO cells, elevations in FBS concentration failed to increase endogenous cholesterol levels in MFN2-KO cells (**Fig. S2D-E**). Likewise, stimulation of ACAT1 by incubation with increasing concentrations of cholesterol (**Fig. S2F**) or with oleic acid (**Fig. S2G**) was unable to stimulate cholesterol esterification in MAM-deficient models as measured by fluorescent cholesterol uptake or lipidomics (**Fig. S2F-G**). In agreement, compared to control levels, exposing

MFN2-KO cells to increasing concentrations of cholesterol failed to induce MAM activity (**Fig. 3E**). Conversely, treating these cells with SMase partially recovered MAM activities (**Fig. 3F**).

Our results show that the modulation of MAM contributes to the uptake of exogenous cholesterol through a yet unknown mechanism. Altogether, these data unveil a crosstalk between the plasma membrane (PM) and MAM, whereby each cellular compartment senses changes in cholesterol levels in the other.

The formation of MAM induces SR-B1-mediated uptake of cholesterol from HDL-particles.

Our data show that MAM formation represses the expression and processing of SREBP2, the master regulator of the expression of cholesterol biosynthesis enzymes, and of LDL-lipoprotein receptors, such as LDLR (43). Therefore, it is possible that the stimulation of cholesterol uptake in cells where MAM is upregulated is a consequence of the sustained inhibition of SREBP2 pathways (27). To determine if this is the case, we overexpressed a transcriptionally-active form of SREBP2 in PS-DKO cells, in which MAM is constitutively activated and HMGCR activity is downregulated. However, we did not observe any effect on the internalization of cholesterol or the activity of the MAM-resident enzyme ACAT1 (**Fig. S3A-D**). This led us to conclude that MAM stimulates cholesterol internalization through a SREBP2-independent pathway.

To explore this further, we quantified the gene expression levels of lipoprotein receptors sensitive to MAM modulation in SMase-treated SH-SY5Y (**Fig. 4A**) and PS-DKO and MFN2-KO cells (**Fig. 4B**). Our results showed that canonical lipoprotein receptors, such as LDLR (low-density lipoprotein receptor) and LRP1 (LDL-related protein 1), were either reduced or not significantly changed by the stimulation or inhibition of MAM formation (**Fig. 4A-B**). Conversely, the expression of the scavenger receptor B1 (SR-B1, gene *SCARB1*) (12), known for its high affinity for HDL particles, was significantly increased upon SMase treatment (**Fig. 4A**). SR-B1 expression was also increased in PS-DKO cells compared to controls and MAM-deficient cells (**Fig. 4B-C and S4A**), however, the levels of this receptor in the PM were either reduced or unchanged in these cell models, as detected by surface biotinylation or giant plasma membrane vesiculation (**Fig. 4D and S4B**).

We further assessed SR-B1's contribution to cholesterol uptake and its PM-ER transfer by incubating SMase-treated cells, as well as PS-DKO cells, with 10 μ M BLT1 (block lipid transport-1), an inhibitor of SR-B1. BLT1 interacts irreversibly with the Cys348 residue of SRB1, impairing its ability to uptake cholesterol, although HDL interaction with SRB1 is enhanced (44). In all of these conditions, SR-B1 inhibition prevented the upregulation of cholesterol uptake, its esterification, and subsequent lipid droplet formation (**Fig. 5A-B and S5A-C**) without affecting cholesterol efflux (**Fig. S5D**). BLT1 treatment also rescued the SMase-induced expression of *SCARB1* and of cholesterol biosynthesis enzymes (**Fig.**

S5E-F). Moreover, SR-B1 inhibition reduced MAM activation (**Fig. 5C**) and the degree of ER-mitochondria apposition (**Fig. S5G**). Additionally, this treatment effectively blocked the expected increase in cholesterol transport to the ER after boosting its levels in the PM by incubation with methyl- β -cyclodextrin (M β CD)-cholesterol complexes (**Fig. S5H**).

Our results suggest that cholesterol uptake via SR-B1, but not by other canonical lipoprotein receptors, contributes to its delivery to the ER and the formation of MAM, although we could not relate this to higher levels of PM SR-B1. However, previous evidence had suggested that the use of cholesterol analogs, such as fluorescent NBD-cholesterol, favor the uptake of these molecules through scavenger receptors, and thus overestimate the involvement of these receptors (45). Therefore, we then decided to evaluate the impact of cholesterol uptake through different types of lipoproteins on the activation of MAM.

SR-B1's strong preference for binding and importing HDL, which is rich in cholesterol esters, opens up the possibility that HDL contributes to the activation of MAM. To test this idea, we measured the levels of cholesterol in WT cells incubated with purified HDL, LDL, or very-low density lipoparticles (VLDL), and compared these levels to WT or PS-DKO cells exposed to complete medium (containing 5% FBS). As observed previously (11, 70), addition of HDL to the medium, but not with LDL or VLDL, induced higher rates of cholesterol influx, compared to what is observed in PS-DKO cells. Similar to our previous data, this was prevented in the presence of BLT1 (**Fig. 6A-B and S6A**). Notably, incubation with different lipoprotein particles had a significant impact on the distribution of cholesterol in cellular membranes as detected by filipin staining (**Fig. 6C and S6B**). Specifically, incubation with LDL and VLDL appeared to expand cholesterol levels in the PM compared to intracellular membranes, resembling cholesterol distribution in MFN2-KO cells (**Fig. S6A-B**). On the other hand, cells incubated with HDL particles displayed increases in intracellular levels of cholesterol compared to PM (**Fig. 6C and S6A-B**), as it occurs in PS-DKO cells (**Fig. 6C**).

Finally, and in line with our previous results, addition of HDLs to the medium induced the activation of MAM-resident enzymes and ER-mitochondria communication, as measured by phospholipid transfer (**Fig. 6D**) and SMase activity (27) (**Fig. S6C**), whereas incubation with LDL or VLDL particles did not affect MAM regulation over control levels. Our data therefore indicates that MAM formation is preferentially stimulated by SRB1-mediated cholesterol uptake from HDL particles, compared to other lipoproteins of lower density. Taken together, our results suggest that MAM formation acts as a cholesterol-sensing mechanism in the ER, reflecting changes in cholesterol levels in the PM and orchestrating feedback reactions to maintain cholesterol homeostasis. We also show that MAM is sensitive to the extracellular lipoprotein environment, thereby contributing to the regulation of cellular metabolic flexibility.

DISCUSSION

Cholesterol regulation is a crucial aspect of maintaining the integrity and function of mammalian cellular membranes. Abnormalities in cholesterol distribution are linked to various pathological conditions, including cardiovascular and neurodegenerative disorders. However, despite significant advancements in this field, some of the mechanisms underlying the complex regulation of cholesterol remain unresolved. For example, it is well established that cholesterol sensing is dependent on specific domains in the endoplasmic reticulum (ER), but the precise identity of these domains is still unknown. Additionally, the mechanisms by which LDL- and HDL-derived cholesterol influence cellular metabolism are not yet fully understood. Our work here indicates that HDL-cholesterol, but not LDL-cholesterol, is delivered to the ER where it induces the formation of MAM domains, stimulating cholesterol esterification and inhibiting *de novo* cholesterol biosynthesis (**Fig. 7**). Our results help characterize MAM as a cholesterol-sensing domain in the ER and support its formation as a key mechanism mediating the distinct metabolic responses of the cell to HDL-derived cholesterol influx.

Cholesterol levels in cellular and intracellular membranes form a gradient maintained by a complex network of mechanisms that balance lipoprotein uptake and biosynthesis, including the control of the expression, compartmentalization and allosteric modulation of the implicated enzymes and proteins (2).

To maintain this network, cholesterol cycles between the PM and the ER. In the ER, the newly-delivered cholesterol elicits feed-back pathways in response to cellular demands (9). Several factors have been revealed to mediate PM-ER cholesterol transport (e.g., Aster/GRAMD or OSBP proteins) (6, 46, 47), especially after SMase treatment (48, 49). However, the complete mechanisms of the sensing of cholesterol accessibility and the regulation of cholesterol PM-to-ER transport are still unclear (50).

The essential role of specific pools of cholesterol in the ER, sensitive to changes in PM, and with high rates of cholesterol esterification activity, has been widely reported in the regulation of this route (9, 18, 23). Relevant to this, the seminal work of Brown and Goldstein (51) demonstrated that these ER cholesterol regulatory pools allosterically modulate cholesterol biosynthesis enzymes and lipoprotein metabolism, primarily via the cleavage and expression of the sterol-regulatory element binding proteins -1 and -2 SREBP1 (gene *SREBF1*) and SREBP2 (gene *SREBF2*) (7, 9). Moreover, multiple reports demonstrate that these cholesterol pools are highly stimulated by treatment with SMase (10, 18, 49).

Based on the abovementioned characteristics, it is evident that MAM domains are equivalent to these pools, which are formed as a consequence of an excess of cholesterol in the PM being delivered to the ER; thus, MAM is known to be highly sensitive to changes in the lipid environment in cellular membranes. Additionally, MAM is a lipid raft-like domain that induces partitioning within ER membranes, resulting in the segregation and allosteric modulation of enzymes involved in the removal of cholesterol by esterification (by ACAT1; *SOAT1*) (27, 39), and oxidation (by CYP46A1) (52). Furthermore, as previously shown for the intracellular pools of cholesterol, MAM is stimulated by sphingomyelin hydrolysis and by incubation with HDL particles. We also show here that MAM formation inhibits the

biosynthesis of cholesterol, and that in agreement with others (32), MAM contains detectable levels of the rate-limiting enzyme HMGCR and is enriched in enzymes comprising the post squalene pathway of cholesterol biosynthesis.

The mevalonate pathway splits into different branches for the production of various metabolites such as isoprenoids, coenzyme Q and cholesterol (2, 7). Channeling of metabolites through one route or the other is highly controlled by rate-limiting enzymes that are regulated pre- and post-transcriptionally and translationally, as well as allosterically by cholesterol levels in cellular membranes (53, 54). For example, HMGCR channels the initial steps of the mevalonate pathway towards the synthesis of farnesyl pyrophosphate (FPP), while SQLE commits the pathway to the synthesis of cholesterol (55). HMGCR and SQLE have been shown to localize in different compartments (2). HMGCR and other enzymes involved in FPP synthesis have been found in peroxisomes, ER, cytosol and mitochondria (2, 56). On the other hand, there is consensus that the post-squalene enzymes are located solely in the ER, where their activity is regulated by cholesterol levels and by SQLE (57, 58), independently of the rest of the mevalonate pathway (21, 33, 55). Therefore, our data highlights the possibility that the formation of MAM specifically enables the compartmentalization and downregulation of the enzymatic branch that produces cholesterol, steering metabolites towards the other branches through organelle contact sites, such as mitochondria (59). In support of this view, MAM formation controls the shunting of cholesterol for the synthesis of steroids in mitochondria (60, 61, 62). Moreover, MAM formation links cholesterol distribution to the modulation of mitochondria and cellular bioenergetics (60, 63, 64)

The contribution of MAM domains to cholesterol metabolism can also be mediated by the regulation of ERLIN2 (36), whose affinity for cholesterol is essential in maintaining the lipid raft structure. ERLIN2 has been shown to repress cholesterol biosynthesis by inhibiting the SREBP2 pathway and by degrading cholesterol biosynthesis enzymes (65, 66). In agreement, a recent publication (41) showed that the loss of ERLIN 1/2 activated SREBP2 pathways, cholesterol synthesis and ER-to-Golgi transport. These data are consistent with the finding that the ablation of ERLIN2 disrupts MAM structure (67). However, under these conditions, the authors also observed the activation of ACAT1 and the production of cholesterol esters and triglycerides (41), perhaps implying that not all MAM activities are inhibited by the elimination of ERLIN2.

Taken together, we conclude that MAM domains facilitate the transient compartmentalization of cholesterol metabolic routes in response to changes in the lipid composition of the PM and also help orchestrate the complex modulation of the cholesterol biosynthesis machinery. Naturally, other cholesterol-rich areas in the ER could also form similar functional domains to facilitate cholesterol modulation and/or the crosstalk with organelles other than the mitochondria (e.g., Golgi) (20, 41, 68).

Our data indicate that exposure to HDL particles induces higher rates of cholesterol internalization and MAM activation in the cell compared to LDL or VLDL particles. It is well known that HDL-rich

environments promote cholesterol influx and efflux from cells (69), in a process involving the ATP-binding cassette (ABC) transporters (70). As a result, compared to other lipoproteins, HDL incubation is associated with a significant downregulation of cholesterol biosynthesis (11). The reason(s) behind differences in the impact of LDL- and HDL-derived cholesterol on the formation of MAM and the inhibition of cholesterol biosynthesis need further investigation. One possibility is that the higher degree of cholesterol transfer induced by HDL via SR-B1, which forms a hydrophobic channel for CEs to move down a concentration gradient from HDL towards cell membranes (12), could stimulate PM-ER transfer in a faster manner relative to LDL particles (71). The dynamics of the mobilization and replenishment of cholesterol pools in the PM are likely distinct in response to HDL-derived cholesterol compared to LDL-derived cholesterol, potentially explaining the varying effects of these lipoprotein particles on the membrane properties (8).

It is also possible that the rapid mobilization of cholesterol from PM to ER induced by HDL can better sustain the formation of lipid-raft domains like MAM within the ER, whereas LDL-induced cholesterol internalization and transport to the ER results in alternate non-raft domains, with distinct impacts on cholesterol biosynthetic activity and on SREBP-mediated pathways. Of note, the capacity of cholesterol to form a lipid raft depends on its association with other lipids such as sphingomyelin. Interestingly, compared to other lipoproteins, HDLs are enriched in sphingomyelin (72).

These distinctive effects on HDLs on cellular cholesterol trafficking may also be attributable to HDLs having higher CE content than LDLs or VLDLs do. It bears mentioning that HDL particles vary in size and composition, thereby impacting cell metabolism in different manners that cannot be solely based on their enrichment in CE content. This has given rise to the suggestion that the HDL subtype, rather than the total CE concentration, has a more critical role in determining this lipoprotein's functional effects (73).

The expression of SR-B1 and the activation of HDL uptake is regulated by several pre- and post-transcriptional mechanism(s) (74, 75) that are highly sensitive to the extracellular environment (76) and that mirror those of LDLR and other SREBP-2-regulated genes (77, 78). Therefore, we propose a model where the formation of the MAM is an essential step in the modulation of the SR-B1-HDL cholesterol pathway that results in the inhibition of SREBP2, although we cannot exclude other receptors implicated in the uptake of these lipoprotein particles. Additionally, we cannot disregard the contribution of other organelle contacts with the ER in the regulation of lipoprotein uptake, such as the PM (e.g., PM-associated ER membranes, or PAM).

Overall, these findings imply that the formation of MAM is sensitive to changes in the extracellular lipid milieu and underlies a mechanism for the translation of exogenous cues into metabolic adjustments. Taken together, our data support the idea that the compartmentalization of cholesterol enzymes into different organelle membranes contributes to the complex regulation of cholesterol metabolism. This hypothesis also implicates the formation of specific domains, such as MAM, as an

essential regulatory step in the channeling of mevalonate metabolites into different pathways and facilitating feed-back mechanism(s) to maintain cholesterol homeostasis and enable cellular responses to changes in the environment.

MATERIAL AND METHODS

Reagents

All reagents, equipment and catalog numbers are listed in the Resources Table.

Cells and animals

SH-SY5Y cells were obtained from the American Type Culture Collection. WT and PSEN1/2-double knock-out (called PS-DKO) mouse embryonic fibroblasts (MEFs) were kind gifts from Dr. Bart De Strooper (University of Leuven). Mfn2-knock-out (MFN2-KO) MEFs, as well as the relevant control MEFs, were kind gifts from Dr. David Chan (California Institute of Technology). Brains from C57BL/6J mice were obtained by cervical dislocation under the approval of the Institutional Animal Care and Use Committee of the Columbia University Medical Center.

Cell treatments

Cells were treated with 1 U/mL SMase. Water-soluble cholesterol (complexed with methyl- β -cyclodextrin) was reconstituted and used at different concentrations as indicated. Oleic acid was used to promote cholesterol esterification. Cells were incubated with 5 ng/mL purified lipoproteins (HDL, LDL, VLDL) in serum-free DMEM. All inhibitors were added for 60min in DMEM supplemented with 5% FBS unless otherwise stated and DMSO was used as a vehicle. 10 μ M BLT1 was used to block the cholesterol transporter SR-B1. Neutral SMase and acidic SMase activities were inhibited with 5 μ M GW4869 or 10 μ M desipramine, respectively. HMGCR activity was blocked using 20 μ M atorvastatin. Cholesterol trafficking via NPC1/Aster was inhibited with 1 μ M U18666A.

Cholesterol trafficking and esterification assays

Cholesterol trafficking and esterification were assessed following established protocols (26). Cells were cultured in serum-free medium for 2 hours to eliminate exogenous lipid interference. Then, 2.5 μ Ci/mL of 3 H-cholesterol was added to serum-free DMEM supplemented with 2% fatty acid-free BSA and allowed to equilibrate at 37°C for at least 30 minutes. In select experiments, the same amount of 3 H-cholesterol was complexed with methyl- β -cyclodextrin. The radiolabeled mixture was then administered to the cells for the specified durations. Afterward, cells were rinsed and harvested in PBS. For some experiments, subcellular fractionation was performed prior to lipid extraction, saving a small aliquot for protein quantification. Equal protein amounts were used to extract lipids by using three volumes of

chloroform:methanol (2:1 v/v). Following vortexing and centrifugation at 8,000 g for 5 minutes, the organic phase was dried under nitrogen. The resulting lipid residue was reconstituted in 30 μ L of chloroform:methanol (2:1 v/v) and applied to a thin-layer chromatography (TLC) plate alongside unlabeled standards. A solvent mixture of hexanes/diethyl ether/acetic acid (80:20:1 v/v/v) was used for TLC. Iodine-stained bands corresponding to cholesterol and cholesteryl esters were scraped off and quantified.

Cholesterol efflux

Cells were loaded with 2.5 mCi/mL of 3 H-cholesterol prepared as described above. Three hours after incubation, cells were washed to remove the excess of exogenous radioactive cholesterol and incubated in unlabeled media in the presence or absence of the indicated inhibitors. After the indicated post-incubation times, media was recovered, briefly centrifuged at 1,500 g for 5 min to remove any debris, transferred to scintillation vials containing 5 mL of scintillation cocktail and radioactivity was measured in a Scintillation Counter.

Cholesterol and lipid droplets staining

1 μ M of the fluorescent cholesterol analog NBD-cholesterol (22-(N-(7-nitrobenz-2-oxa-1,3-diazol-4-yl)amino)-23,24-bisnor-5-cholen-3 β -ol) was used to determine cholesterol uptake. Filipin staining was performed after 4% paraformaldehyde fixation by incubation with 50 mg/mL of filipin for 2 h at room temperature. Staining of lipid droplets was performed using HCS LipidToxTM Green following manufacturer instructions. After extensive washes, coverslips were mounted with Fluoromount-GTM and visualized by confocal fluorescence microscopy. Staining was quantified using ImageJ. Reported fluorescence intensity represents the product of the intensity and the area covered by the fluorescent signal above background in every cell examined. In some experiments, DAPI was used to visualize nuclei.

In some experiments, the protocol was adapted to a multi-well format and the fluorescence intensity was measured using specific settings and bandwidths in a multi-plate reader.

HMG-CoA reductase (HMGCR) activity assay

HMGCR activity was measured following manufacturer instructions from equal protein amounts.

Phospholipid transfer

2.5 μ Ci/mL 3 H-serine was added to the cells for the specified time-points. In some experiments, drugs were added immediately before 3 H-serine incubation, unless otherwise indicated. After extensive washing, cells were collected and lipids extracted and separated by TLC as detailed in (29). Incorporation of 3 H-serine into phosphatidylserine (PS) and phosphatidylethanolamine (PE) was measured.

Sphingomyelinase activity assay

Cells were incubated with 1 μ M sphingomyelin C16-Cy5 for 3 h at 37°C. After extensive washing, cells were collected and the organic and the aqueous phases were separated by mixing the sample with chloroform:methanol:H₂O (2:1:1), followed by centrifugation at 8,000 g for 5 min. The aqueous phase, containing fluorescent phosphocholine, was collected and fluorescence measured (excitation/emission, 640/685 nm, bandwidth 30 nm) in a plate reader.

Subcellular fractionation

Purification of ER, crude membranes (CM), mitochondria and MAM was performed and analyzed as described (26).

Western blotting

After quantification of sample protein concentrations via BCA assay, equal amounts of protein were boiled in Laemmli sample buffer and run in 4-20% Tris-glycine gels. Proteins were detected using the antibodies listed in the Reagents Table.

Analysis of ER-mitochondria apposition

Cells were co-transfected with mCherry-SEC61B (Addgene plasmid, #90994) and mitoGFP (Addgene plasmid, #159096) at a 1:1 ratio using Lipofectamine™ 2000 Transfection Reagent in serum-free DMEM for 4-6 h following manufacturer instructions. 16 h post-transfection, cells were treated with SMase or BLT1 for 1 h or 3 h, images of double-transfected cells were acquired, and ER-mitochondria apposition was analyzed as described (27).

Transient expression of the mature form of SREBP2

PS-DKO cells were transfected with the truncated mature form of SREBP2 (2xFLAG-SREBP2, aa 1-482, Addgene plasmid #26807), which is targeted to the nucleus where it activates cholesterol biosynthesis gene programs. 16 h post-transfection, cells were assayed for cholesterol uptake and esterification, as well as protein expression of 2xFLAG-SREBP2.

Labeling and purification of plasma membrane proteins

Plasma membrane proteins were biotinylated by incubation with 1 mg/mL of EZ-Link™ Sulfo-NHS-LC-Biotin in labeling buffer (20 mM HEPES, 150 mM NaCl, 2 mM CaCl₂, pH 8.5) at 4°C for 45 minutes under dark conditions. Subsequent washing steps with PBS containing glycine were conducted to quench unreacted biotin. Cells were then lysed in 50 mM Tris pH 7.5, 5 mM EGTA, 10 mM EDTA supplemented with protease inhibitors by sonication and addition of 1% sodium deoxycholate. After centrifugation, the supernatant containing the lysate was collected, and a fraction was reserved as input. Streptavidin-coated beads, pre-washed in 50 mM Tris pH 7.5, were added to the lysate and incubated

overnight at 4°C. Following extensive washing, the bound proteins were eluted by heating at 45°C in 1xLaemmli buffer to prevent protein aggregation.

Generation of Giant Plasma Membrane Vesicles

GPMVs were generated by washing the cells in 10 mM HEPES, 150 mM NaCl, 2 mM CaCl₂, pH 7.4, and treatment with 2 mM N-ethylmaleimide for 1 h at 37 °C. The suspension containing the GPMVs was centrifuged at 500 g for 5 min to eliminate cellular debris and GPMVs were collected by centrifugation at 20,000 g for 1 h. GPMVs were quantified via BCA assay and processed for western blot analysis.

Quantitative reverse transcription–polymerase chain reaction (qRT–PCR)

Total RNA was extracted using TRIzol[®] Reagent according to the manufacturer's instructions and was quantified by NanoDrop2000. One microgram of total RNA was used to generate cDNA by RT–PCR using the High-Capacity cDNA Reverse Transcription Kit. Quantitative Real-Time PCR was performed in triplicate in a StepOnePlus™ Real-Time PCR System. The expression of each gene under study was analyzed using specific predesigned TaqMan Probes (see Reagents Table) and normalized against 18S rRNA expression as an internal control.

Lipidomics analysis

Lipids were extracted from equal amounts of material (30 mg protein/sample). Lipid extracts were prepared via chloroform–methanol extraction, spiked with appropriate internal standards, and analyzed using a 6490 Triple Quadrupole LC/MS system as described previously (83). Different lipid classes were separated with normal-phase HPLC using an Agilent Zorbax Rx-Sil column (inner diameter 2.1 Å~ 100 mm) under the following conditions: mobile phase A (chloroform:methanol:1 M ammonium hydroxide, 89.9:10:0.1, v/v/v) and mobile phase B (chloroform:methanol:water:ammonium hydroxide, 55:39.9:5:0.1, v/v/v/v); 95% A for 2 min, linear gradient to 30% A over 18 min and held for 3 min, and linear gradient to 95% A over 2 min and held for 6 min. Quantification of lipid species was accomplished using multiple reaction monitoring (MRM) transitions that were developed in earlier studies in conjunction with referencing of appropriate internal standards. Values were represented as mole fraction with respect to total lipid (% molarity). For this, the lipid mass of any specific lipid was normalized by the total mass of all the lipids measured.

Analysis of PhotoClick cholesterol-interacting proteome in MAM fractions

Cholesterol-interacting proteins from MAM fractions were pulled down employing a Photoclick cholesterol analog (Hex-5'-ynyl 3β-hydroxy-6-diaziriny-5α-cholan-24-oate), as detailed in (27). Briefly, 5 μM PhotoClick cholesterol was incubated with MEFs for 4 h. Upon extensive washing, PhotoClick cholesterol was crosslinked under 365nm-UV, and cells were collected for subcellular fractionation. 500

μg of MAM fractions were briefly sonicated and subjected to click chemistry by addition of 500 μM biotin-azide, 100 μM Tris((1-benzyl-4-triazolyl)methyl)amine (TBTA), 1 mM CuSO_4 and 1 mM Tris(2-carboxyethyl)phosphine (TCEP) and incubation for 15 min at room temperature in the dark. Then, streptavidin beads were used to pull down biotinylated cholesterol-interacting proteins. Upon several washes, samples for proteomic analysis were snap-frozen and stored at -80°C for downstream proteomic analysis.

Label-free quantitative proteomic profiling and analysis were performed at the Proteomics Shared Resource at Columbia University Medical Center as reported in (84).

Statistical analysis

Data represent mean \pm SEM. All averages are the result of three or more independent experiments, carried out at different times with different sets of samples. Data distribution was assumed to be normal. The statistical analysis was performed using GraphPad Prism v9.01. Brown-Forsythe test was used to compare variance between groups. Statistical significance was determined by either two-tailed t-test or (repeated measures) two-way ANOVA, followed by the Tukey's or Sidak's multiple comparison post-hoc test. Welch's corrections were used for t-test comparison when variance between groups was statistically different, as stated. Values of $p < 0.05$ were considered statistically significant. * $p < 0.05$, ** $p < 0.01$, *** $p < 0.001$, **** $p < 0.0001$. The investigators were not blinded when quantifying imaging experiments.

Acknowledgements.

This work was supported by the U.S. National Institutes of Health (R01-AG056387-01 to E.A.-G.; T32-DK007647 to RRA and KAT; R01-NS117538 to EAS), the U.S. Department of Defense (FA9550-11-C-0028 to RRA), the Spanish Ministry of Science, Innovation and Universities (PID2021-126818NB-I00 to EA-G; FPI fellowship PRE2022-104771 to ACF; FPU fellowship 22/00245 to MU) and the European Union's Horizon 2020 research and innovation programme under the Marie Skłodowska-Curie grant agreement (MSCA-PF 101106857 to JM).

We thank Renu Nandakumar for assistance with the lipidomics analysis and members of the Columbia University Irving Medical Center for helpful discussions and support.

Author Contributions Statement: Conceived the project: EA-G, EAS and JM. Designed experiments: EA-G, JM, KK and MU. Generated experimental data: EA-G, JM, KK, MU, DL, RRA, MP, ACF, KAT, KRV and NGL. Collected/analyzed lipidomics data: TDY and EA-G. Wrote the manuscript: JM and EA-G. Critically edited the manuscript: all authors. Approved final version of the manuscript: all authors.

Competing interests: The authors declare that they have no competing interests.

Data availability: The mass spectrometry proteomics data have been deposited to the ProteomeXchange Consortium via the PRIDE partner repository with the dataset identifier PXD053417 and 10.6019/PXD053417.

REFERENCES

1. J. Montesinos, C. Guardia-Laguarta, E. Area-Gomez, The fat brain. *Curr Opin Clin Nutr Metab Care* **23**, 68-75 (2020).
2. E. Ikonen, Mechanisms of cellular cholesterol compartmentalization: recent insights. *Curr Opin Cell Biol* **53**, 77-83 (2018).
3. O. A. Isik, O. Cizmecioglu, Rafting on the Plasma Membrane: Lipid Rafts in Signaling and Disease. *Adv Exp Med Biol* **1436**, 87-108 (2023).
4. E. Sezgin, I. Levental, S. Mayor, C. Eggeling, The mystery of membrane organization: composition, regulation and roles of lipid rafts. *Nat Rev Mol Cell Biol* **18**, 361-374 (2017).
5. K. Simons, W. L. Vaz, Model systems, lipid rafts, and cell membranes. *Annu. Rev. Biophys. Biomol. Struct.* **33**, 269-295 (2004).
6. V. M. Olkkonen, E. Ikonen, Cholesterol transport in the late endocytic pathway: Roles of ORP family proteins. *J Steroid Biochem Mol Biol* **216**, 106040 (2022).
7. J. Luo, L. Jiang, H. Yang, B. L. Song, Routes and mechanisms of post-endosomal cholesterol trafficking: A story that never ends. *Traffic* **18**, 209-217 (2017).
8. A. Das, M. S. Brown, D. D. Anderson, J. L. Goldstein, A. Radhakrishnan, Three pools of plasma membrane cholesterol and their relation to cholesterol homeostasis. *Elife* **3**, (2014).
9. R. E. Infante, A. Radhakrishnan, Continuous transport of a small fraction of plasma membrane cholesterol to endoplasmic reticulum regulates total cellular cholesterol. *Elife* **6**, (2017).
10. S. Endapally *et al.*, Molecular Discrimination between Two Conformations of Sphingomyelin in Plasma Membranes. *Cell* **176**, 1040-1053 e1017 (2019).
11. Q. Zhang, Y. Ke, H. Hong, HDL and Lipid Metabolism. *Adv Exp Med Biol* **1377**, 49-61 (2022).
12. H. Yu, HDL and Scavenger Receptor Class B Type I (SRBI). *Adv Exp Med Biol* **1377**, 79-93 (2022).
13. V. L. Meiner *et al.*, Disruption of the acyl-CoA:cholesterol acyltransferase gene in mice: evidence suggesting multiple cholesterol esterification enzymes in mammals. *Proc Natl Acad Sci U S A* **93**, 14041-14046 (1996).
14. J. Sandhu *et al.*, Aster Proteins Facilitate Nonvesicular Plasma Membrane to ER Cholesterol Transport in Mammalian Cells. *Cell* **175**, 514-529.e520 (2018).
15. J. P. Kennelly, P. Tontonoz, Cholesterol Transport to the Endoplasmic Reticulum. *Cold Spring Harb Perspect Biol* **15**, (2023).
16. J. P. Slotte, E. L. Bierman, Depletion of plasma-membrane sphingomyelin rapidly alters the distribution of cholesterol between plasma membranes and intracellular cholesterol pools in cultured fibroblasts. *Biochem J* **250**, 653-658 (1988).
17. Y. Lange, J. Ye, M. Rigney, T. L. Steck, Regulation of endoplasmic reticulum cholesterol by plasma membrane cholesterol. *J Lipid Res* **40**, 2264-2270 (1999).
18. Y. Lange, T. L. Steck, Quantitation of the pool of cholesterol associated with acyl-CoA:cholesterol acyltransferase in human fibroblasts. *J Biol Chem* **272**, 13103-13108 (1997).

19. Y. Lange, T. L. Steck, The role of intracellular cholesterol transport in cholesterol homeostasis. *Trends Cell Biol* **6**, 205-208 (1996).
20. I. Kristiana, H. Yang, A. J. Brown, Different kinetics of cholesterol delivery to components of the cholesterol homeostatic machinery: implications for cholesterol trafficking to the endoplasmic reticulum. *Biochim Biophys Acta* **1781**, 724-730 (2008).
21. L. J. Sharpe, H. W. Coates, A. J. Brown, Post-translational control of the long and winding road to cholesterol. *J Biol Chem* **295**, 17549-17559 (2020).
22. M. Hao *et al.*, Vesicular and non-vesicular sterol transport in living cells. The endocytic recycling compartment is a major sterol storage organelle. *J Biol Chem* **277**, 609-617 (2002).
23. D. B. Iaea, F. R. Maxfield, Membrane order in the plasma membrane and endocytic recycling compartment. *PLoS One* **12**, e0188041 (2017).
24. L. Scorrano *et al.*, Coming together to define membrane contact sites. *Nat Commun* **10**, 1287 (2019).
25. L. K. Townsend, H. S. Brunetta, M. A. S. Mori, Mitochondria-associated ER membranes in glucose homeostasis and insulin resistance. *Am J Physiol Endocrinol Metab* **319**, E1053-E1060 (2020).
26. M. Pera *et al.*, Increased localization of APP-C99 in mitochondria-associated ER membranes causes mitochondrial dysfunction in Alzheimer disease. *EMBO J* **36**, 3356-3371 (2017).
27. J. Montesinos *et al.*, The Alzheimer's disease-associated C99 fragment of APP regulates cellular cholesterol trafficking. *EMBO J*, e103791 (2020).
28. E. W. Haeffner, U. Wittmann, Cholesterol-induced growth stimulation, macromolecule synthesis, and increased phosphoinositide metabolism of ascites tumour cells in culture. *Cell Signal* **11**, 821-829 (1999).
29. J. Montesinos, E. Area-Gomez, M. Schlame, Analysis of phospholipid synthesis in mitochondria. *Methods Cell Biol* **155**, 321-335 (2020).
30. X. Xiao *et al.*, Selective Aster inhibitors distinguish vesicular and nonvesicular sterol transport mechanisms. *Proc Natl Acad Sci U S A* **118**, (2021).
31. J. J. Hulce, A. B. Cognetta, M. J. Niphakis, S. E. Tully, B. F. Cravatt, Proteome-wide mapping of cholesterol-interacting proteins in mammalian cells. *Nat Methods* **10**, 259-264 (2013).
32. A. Sala-Vila *et al.*, Interplay between hepatic mitochondria-associated membranes, lipid metabolism and caveolin-1 in mice. *Sci Rep* **6**, 27351 (2016).
33. H. Yoshioka *et al.*, A key mammalian cholesterol synthesis enzyme, squalene monooxygenase, is allosterically stabilized by its substrate. *Proc Natl Acad Sci U S A* **117**, 7150-7158 (2020).
34. M. Y. W. Ng *et al.*, The cholesterol transport protein GRAMD1C regulates autophagy initiation and mitochondrial bioenergetics. *Nat Commun* **13**, 6283 (2022).
35. Y. Wang *et al.*, The selective Alzheimer's disease indicator-1 gene (Seladin-1/DHCR24) is a liver X receptor target gene. *Mol Pharmacol* **74**, 1716-1721 (2008).
36. D. T. Browman, M. E. Resek, L. D. Zajchowski, S. M. Robbins, Erlin-1 and erlin-2 are novel members of the prohibitin family of proteins that define lipid-raft-like domains of the ER. *J. Cell Sci.* **119**, 3149-3160 (2006).
37. A. Zhang *et al.*, Quantitative proteomic analyses of human cytomegalovirus-induced restructuring of endoplasmic reticulum-mitochondrial contacts at late times of infection. *Mol Cell Proteomics* **10**, M111 009936 (2011).
38. T. Y. Chang, B. L. Li, C. C. Chang, Y. Urano, Acyl-coenzyme A:cholesterol acyltransferases. *Am. J. Physiol. Endocrinol. Metab.* **297**, E1-E9 (2009).
39. T. C. Harned *et al.*, Acute ACAT1/SOAT1 Blockade Increases MAM Cholesterol and Strengthens ER-Mitochondria Connectivity. *Int J Mol Sci* **24**, (2023).
40. J. Montesinos, E. Area-Gomez, Isolation of mitochondria-associated ER membranes. *Methods Cell Biol* **155**, 33-44 (2020).

41. M. Veronese *et al.*, ERLIN1/2 scaffolds bridge TMUB1 and RNF170 and restrict cholesterol esterification to regulate the secretory pathway. *Life Sci Alliance* **7**, (2024).
42. E. Area-Gomez *et al.*, Upregulated function of mitochondria-associated ER membranes in Alzheimer disease. *EMBO J* **31**, 4106-4123 (2012).
43. B. B. Madison, Srebp2: A master regulator of sterol and fatty acid synthesis. *J Lipid Res* **57**, 333-335 (2016).
44. M. Yu, T. Y. Lau, S. A. Carr, M. Krieger, Contributions of a disulfide bond and a reduced cysteine side chain to the intrinsic activity of the high-density lipoprotein receptor SR-BI. *Biochemistry* **51**, 10044-10055 (2012).
45. A. Frolov *et al.*, High density lipoprotein-mediated cholesterol uptake and targeting to lipid droplets in intact L-cell fibroblasts. A single- and multiphoton fluorescence approach. *J Biol Chem* **275**, 12769-12780 (2000).
46. S. Endapally, R. E. Infante, A. Radhakrishnan, Monitoring and Modulating Intracellular Cholesterol Trafficking Using ALOD4, a Cholesterol-Binding Protein. *Methods Mol Biol* **1949**, 153-163 (2019).
47. C. Zhang *et al.*, OSBPL2 deficiency upregulate SQLE expression increasing intracellular cholesterol and cholesteryl ester by AMPK/SP1 and SREBF2 signalling pathway. *Exp Cell Res* **383**, 111512 (2019).
48. A. Ferrari *et al.*, Aster-dependent nonvesicular transport facilitates dietary cholesterol uptake. *Science* **382**, eadf0966 (2023).
49. T. Naito *et al.*, Movement of accessible plasma membrane cholesterol by the GRAMD1 lipid transfer protein complex. *Elife* **8**, (2019).
50. D. Y. Litvinov, E. V. Savushkin, A. D. Dergunov, Intracellular and Plasma Membrane Events in Cholesterol Transport and Homeostasis. *J Lipids* **2018**, 3965054 (2018).
51. M. S. Brown, J. L. Goldstein, A proteolytic pathway that controls the cholesterol content of membranes, cells, and blood. *Proc Natl Acad Sci U S A* **96**, 11041-11048 (1999).
52. Y. Zhao *et al.*, ATAD3A oligomerization promotes neuropathology and cognitive deficits in Alzheimer's disease models. *Nat Commun* **13**, 1121 (2022).
53. T. Long, E. W. Debler, X. Li, Structural enzymology of cholesterol biosynthesis and storage. *Curr Opin Struct Biol* **74**, 102369 (2022).
54. Q. Shi, J. Chen, X. Zou, X. Tang, Intracellular Cholesterol Synthesis and Transport. *Front Cell Dev Biol* **10**, 819281 (2022).
55. V. Howe, L. J. Sharpe, A. V. Prabhu, A. J. Brown, New insights into cellular cholesterol acquisition: promoter analysis of human HMGCR and SQLE, two key control enzymes in cholesterol synthesis. *Biochim Biophys Acta Mol Cell Biol Lipids* **1862**, 647-657 (2017).
56. W. J. Kovacs, L. M. Olivier, S. K. Krisans, Central role of peroxisomes in isoprenoid biosynthesis. *Prog Lipid Res* **41**, 369-391 (2002).
57. W. A. Prinz, A cholesterol-sensing mechanism unfolds. *J Biol Chem* **292**, 19974-19975 (2017).
58. N. K. Chua, V. Howe, N. Jatana, L. Thukral, A. J. Brown, A conserved degron containing an amphipathic helix regulates the cholesterol-mediated turnover of human squalene monooxygenase, a rate-limiting enzyme in cholesterol synthesis. *J Biol Chem* **292**, 19959-19973 (2017).
59. M. Fujimoto, T. Hayashi, T. P. Su, The role of cholesterol in the association of endoplasmic reticulum membranes with mitochondria. *Biochem. Biophys. Res. Commun.* **417**, 635-639 (2012).
60. P. Elustondo, L. A. Martin, B. Karten, Mitochondrial cholesterol import. *Biochim Biophys Acta Mol Cell Biol Lipids* **1862**, 90-101 (2017).
61. M. Doghman-Bouguerra, E. Lalli, The ER-mitochondria couple: In life and death from steroidogenesis to tumorigenesis. *Mol Cell Endocrinol* **441**, 176-184 (2017).

62. L. Szabo *et al.*, ER-mitochondria contacts and cholesterol metabolism are disrupted by disease-associated tau protein. *EMBO Rep* **24**, e57499 (2023).
63. C. T. J. Wall *et al.*, Mitochondrial respiratory chain dysfunction alters ER sterol sensing and mevalonate pathway activity. *J Biol Chem* **298**, 101652 (2022).
64. P. M. Tricarico, S. Crovella, F. Celsi, Mevalonate Pathway Blockade, Mitochondrial Dysfunction and Autophagy: A Possible Link. *Int J Mol Sci* **16**, 16067-16084 (2015).
65. L. M. Wolf, A. M. Lambert, J. Haenlin, M. Boutros, EVI/WLS function is regulated by ubiquitylation and is linked to ER-associated degradation by ERLIN2. *J Cell Sci* **134**, (2021).
66. M. D. Huber, P. W. Vesely, K. Datta, L. Gerace, Erlins restrict SREBP activation in the ER and regulate cellular cholesterol homeostasis. *J Cell Biol* **203**, 427-436 (2013).
67. V. Manganelli *et al.*, Role of ERLINs in the Control of Cell Fate through Lipid Rafts. *Cells* **10**, (2021).
68. T. Naito *et al.*, Regulation of cellular cholesterol distribution via non-vesicular lipid transport at ER-Golgi contact sites. *Nat Commun* **14**, 5867 (2023).
69. W. J. Shen, S. Azhar, F. B. Kraemer, SR-B1: A Unique Multifunctional Receptor for Cholesterol Influx and Efflux. *Annu Rev Physiol* **80**, 95-116 (2018).
70. N. R. Webb *et al.*, The fate of HDL particles in vivo after SR-BI-mediated selective lipid uptake. *J Lipid Res* **43**, 1890-1898 (2002).
71. N. A. Baumann *et al.*, Transport of newly synthesized sterol to the sterol-enriched plasma membrane occurs via nonvesicular equilibration. *Biochemistry* **44**, 5816-5826 (2005).
72. R. Martínez-Beamonte, J. M. Lou-Bonafonte, M. V. Martínez-Gracia, J. Osada, Sphingomyelin in high-density lipoproteins: structural role and biological function. *Int J Mol Sci* **14**, 7716-7741 (2013).
73. E. Tubbs *et al.*, Sulforaphane improves disrupted ER-mitochondria interactions and suppresses exaggerated hepatic glucose production. *Mol Cell Endocrinol* **461**, 205-214 (2018).
74. A. P. Kent, I. M. Stylianou, Scavenger receptor class B member 1 protein: hepatic regulation and its effects on lipids, reverse cholesterol transport, and atherosclerosis. *Hepat Med* **3**, 29-44 (2011).
75. H. A. B. Paterson *et al.*, Liver RBFOX2 regulates cholesterol homeostasis via Scarb1 alternative splicing in mice. *Nat Metab* **4**, 1812-1829 (2022).
76. R. A. Srivastava, Scavenger receptor class B type I expression in murine brain and regulation by estrogen and dietary cholesterol. *J Neurol Sci* **210**, 11-18 (2003).
77. A. Michihara, M. Mido, H. Matsuoka, Y. Mizutani, Lower Squalene Epoxidase and Higher Scavenger Receptor Class B Type 1 Protein Levels Are Involved in Reduced Serum Cholesterol Levels in Stroke-Prone Spontaneously Hypertensive Rats. *Biol Pharm Bull* **38**, 1879-1890 (2015).
78. W. J. Shen, S. Asthana, F. B. Kraemer, S. Azhar, Scavenger receptor B type 1: expression, molecular regulation, and cholesterol transport function. *J Lipid Res* **59**, 1114-1131 (2018).
79. J. Herms *et al.*, Cortical dysplasia resembling human type 2 lissencephaly in mice lacking all three APP family members. *EMBO J* **23**, 4106-4115 (2004).
80. E. Area-Gomez, Assessing the function of mitochondria-associated ER membranes. *Methods Enzymol* **547**, 181-197 (2014).
81. C. Guardia-Laguarta *et al.*, alpha-Synuclein is localized to mitochondria-associated ER membranes. *J Neurosci* **34**, 249-259 (2014).
82. E. Area-Gomez *et al.*, Lipidomics study of plasma from patients suggest that ALS and PLS are part of a continuum of motor neuron disorders. *Sci Rep* **11**, 13562 (2021).
83. R. B. Chan *et al.*, Comparative lipidomic analysis of mouse and human brain with Alzheimer disease. *J Biol Chem* **287**, 2678-2688 (2012).

84. J. Chen *et al.*, Juvenile CLN3 disease is a lysosomal cholesterol storage disorder: similarities with Niemann-Pick Type C disease. *EBioMedicine* **92**, 104628 (2023).

FIGURE LEGENDS

Fig. 1. Cholesterol internalization and delivery to the ER induces MAM activity

A,B. ^3H -cholesterol internalization (**A**) and esterification (**B**) induced by increasing concentrations of exogenously added cholesterol in SH-SY5Y cells.

C. MAM activity measured as the incorporation of ^3H -serine into phosphatidylserine (PS) and phosphatidylethanolamine (PE) in SH-SY5Y cells exposed to increasing concentrations of cholesterol.

D. Filipin staining of cells treated with or without sphingomyelinase (SMase, 1 U/mL) for 2h. Scale bar= 20 μm .

E. ^3H -cholesterol internalization and its esterification in cells exposed to SMase treatment.

F. ^3H -serine incorporation into PS or PE in cells treated with SMase (1 U/mL) or the SMase inhibitor GW4869 (5 μM).

Fig. 2. Cholesterol uptake inhibits cholesterol biosynthesis

A. HMGCR activity and mRNA expression levels in SH-SY5Y cells exposed or not to 1U/mL SMase for 3 h.

B. Protein levels of cholesterol biosynthetic enzymes obtained by proteomics analysis of cholesterol-interacting targets from MAM isolated from mouse fibroblasts. Data are presented as the \log_2 of the normalized average total ion current. The biosynthetic pathway of cholesterol is depicted in the diagram and enzymes identified in the PhotoClick-cholesterol proteomics assay are underlined. HMGCR: 3-hydroxy-3-methylglutaryl-coenzyme A reductase; FDFT1: squalene synthase; SQLE: squalene monooxygenase; LSS: lanosterol synthase; CYP51A1: lanosterol 14-alpha demethylase, TM7SF2: delta(14)-sterol reductase; MSMO1: methylsterol monooxygenase 1; NSDHL: sterol-4-alpha-carboxylate 3-dehydrogenase; HSD17B7: 17-beta-hydroxysteroid dehydrogenase 7; DHCR24: delta(24)-sterol reductase; EBP: 3-beta-hydroxysteroid-Delta(8),Delta(7)-isomerase; SC5D: lathosterol oxidase; DHCR7: 7-dehydrocholesterol reductase; SOAT1: Sterol O-acyltransferase 1 (ACAT1); ACSL4: Long-chain-fatty-acid--CoA ligase 4 (FACL4).

C. Western blot detection of cholesterol biosynthetic enzymes in different subcellular fractions obtained from mouse brain. TH: total homogenate. CM: crude membranes. MIT: mitochondria. CYT: cytosol (representative of 3 independent experiments). Sizes, in kDa, at left.

Fig. 3. MAM controls cholesterol uptake

- A.** Representative images of cells with chronic MAM upregulation (PS-DKO) or MAM deficiency (MFN2-KO) incubated with fluorescent cholesterol (NBD-cholesterol, green arrows) for 1 h and stained with filipin to detect endogenous cholesterol (blue arrows). Scale bar = 20 μ m.
- B,C,D.** Quantification of NBD-cholesterol uptake (**B**), HMGCR activity (**C**) and mRNA levels of *Hmgcr* (**D**) in PS-DKO, MFN2-KO and wild-type (WT) counterpart MEF cells.
- E.** 3 H-serine incorporation into PS or PE in MAM-deficient and control cells exposed to increasing concentrations of cholesterol.
- F.** 3 H-serine incorporation into PS or PE in MAM-deficient or control cells treated with SMase (1 U/mL).

Fig. 4. MAM regulates cholesterol uptake via the activation of SR-B1

- A,B.** mRNA expression levels of cholesterol transporters in (**A**) SH-SY5Y cells exposed to SMase (1U/mL, 3 h) and (**B**) PS-DKO and MFN2-KO cells and their WT counterparts.
- C,D.** Quantification of total (**C**) or plasma membrane (**D**) protein levels of LRP1 and SR-B1 in PS-WT and PS-DKO cells. Tubulin was used as a loading control for total homogenates and Na⁺/K⁺ ATPase (ATP1A1) as a control for plasma membrane purification. Representative immunoblots are shown. Sizes, in kDa, at left.

Fig. 5. Blocking SR-B1-dependent cholesterol uptake inhibits MAM activities

- A.** Pretreatment with the SR-B1 inhibitor BLT1 (10 μ M, 30 min) prevents the SMase-induced increase in NBD-cholesterol uptake. Representative images are shown; the quantification of NBD-cholesterol fluorescence per cell at right.
- B.** BLT1 reduces NBD-cholesterol uptake in PS-WT and PS-DKO cells. Representative images are shown and the quantification of NBD-cholesterol fluorescence per cell.
- C.** 3 H-serine incorporation into PS and PE in PS-WT and PS-DKO cells treated with BLT1 (10 μ M) immediately before addition of 3 H-serine.

Fig. 6. HDL-cholesterol uptake induces MAM activation

- A-C.** (**A**) Filipin staining of PS-WT cells incubated in either 10% FBS without added lipoproteins (\emptyset) or in serum-free medium with 5ng/ml of different lipoproteins (HDL, LDL, VLDL) for 5 h, in the presence or absence of BLT1 (10 μ M). Filipin staining of PS-DKO cells in 10% FBS treated or not with BLT1 are also shown. Scale bar = 10 μ m. (**B**) Quantification of filipin puncta per cell and (**C**) filipin intensity present at the cytosol or around the plasma membrane, corrected by the area of the region.
- D.** 3 H-serine incorporation into PS or PE in cells incubated with 5% FBS or lipoproteins for 5 h. The exposure to 2.5Ci/mL 3 H-serine took place during the last 4 h of incubation with FBS or lipoproteins.

Fig. 7. Cholesterol influx from HDL via SR-B1 modulates MAM activities, such as phosphatidylserine transport and conversion into phosphatidylethanolamine and cholesterol esterification, while inhibiting cholesterol synthesis. SMase facilitates cholesterol trafficking towards MAM eliciting similar responses.

Supplementary Figures

Fig. S1.

A, B. ^3H -cholesterol internalization (**A**) and esterification (**B**) induced by increasing concentrations of exogenously-added cholesterol in MEFs.

C, D. MAM activity measured as the incorporation of ^3H -serine into phosphatidylserine (PS) and phosphatidylethanolamine (PE) in MEFs exposed to increasing concentrations of cholesterol.

E. ^3H -cholesterol levels internalized (INT), detected at MAM fractions, and detected at ER fractions in SH-SY5Y cells incubated for 3 h with ^3H -cholesterol and SMase (1U/mL).

F. ^3H -cholesterol internalization and its esterification in MEFs treated with SMase (1 U/mL).

G. ^3H -serine incorporation into PS and PE in mouse fibroblasts exposed to SMase (1 U/mL).

H. ER-mitochondria co-localization in SH-SY5Y cells expressing Sec61B-mCherry and mitoGFP and treated with 1 U/mL SMase. Nuclei were stained with DAPI. ER-mitochondria co-localization shown in gray. Scale bar = 20 μm .

I. ^3H -serine incorporation into PS and PE in cells exposed to SMase with or without the NPC1/Aster inhibitor U18666A (1 μM).

J. ^3H -serine incorporation into PS or PE in SH-SY5Y cells pre-treated with atorvastatin (20 μM) for 16h.

Fig. S2.

A. Quantification of the precursor and mature forms of the cholesterol master regulator SREBP2 after exposure to SMase (1 U/mL, 3 h). Protein levels are normalized to the loading control (β -actin). Sizes, in kDa, at left.

B. mRNA levels of selected components of the cholesterol biosynthesis machinery in SMase-treated cells.

C. ^3H -cholesterol uptake in PS-DKO and MFN2-KO cells over their respective WT counterparts (dotted line).

D. Quantification of fluorescence of cholesterol-stained filipin in PS-DKO and MFN2-KO cells and in their WT counterparts exposed to increasing concentrations of FBS.

E. NBD-cholesterol uptake in PS-WT, PS-DKO, MFN2-WT and MFN2-KO cells in the presence of 1%, 5% and 10% FBS.

F. Lipidomic analysis of MAM-deficient (MFN2-KO) and control cells exposed to 3 mg or 5 mg cholesterol/100mL for 6 h. Data are presented as fold-change (\log_2) over cells treated with 0.5 mg cholesterol/100mL. Colored intensity corresponds to a FDR q -value <0.05 .

G. Imaging of MFN2-WT and MFN2-KO cells exposed to NBD-cholesterol and 0.6 mM of oleic acid for 3 h. Scale bar = 20 μ m.

Fig. S3.

A-C. A FLAG-tagged transcriptionally-active form of the cholesterol master regulator SREBP2 was overexpressed in PS-DKO cells, followed by analysis of NBD-cholesterol uptake (**A**), ^3H -cholesterol internalization (**B**) and its esterification (**C**). Transfection with an empty vector was used as control.

D. A representative immunoblot to detect the mature SREBP2^{FLAG}. β -actin was used as a loading control. Sizes, in kDa, at left.

Fig. S4

A. Quantification of SR-B1 in total homogenates of MFN2-WT and MFN2-KO cells. β -actin was used as a loading control. A representative immunoblot is shown. Sizes, in kDa, at left.

B. Quantification of SR-B1 in plasma membrane, obtained as giant plasma membrane vesicles (GPMV) from PS-DKO, MFN2-KO and their WT counterparts. ATP1A1 was used as a plasma membrane loading control. A representative immunoblot is shown. Sizes, in kDa, at left.

Fig. S5.

A. Representative images of lipid droplet staining with LipidTOXTM in PS-WT and PS-DKO cells treated with 10 μ M of BLT1 for 16 h. Quantitation at left.

B,C. ^3H -cholesterol uptake and esterification into cholesteryl-esters (CE) in BLT1-treated PS-WT (**B**) or PS-DKO (**C**) cells.

D. PS-DKO cells were loaded with ^3H -cholesterol for 3h and, following extensive washing, ^3H -cholesterol efflux was monitored in the presence of BLT1.

E,F. mRNA levels of selected components of the cholesterol biosynthetic machinery (**E**) and the cholesterol transporter *SCARB1* (**F**) were analyzed in SH-SY5Y cells exposed to 1U/mL SMase and/or 10 μ M BLT1 for 3 h.

G. ER-mitochondria co-localization in SH-SY5Y cells expressing Sec61B-mCherry and mitoGFP and exposed to 1 U/mL SMase and/or 10 μ M BLT1 for 3 h. Nuclei were stained with DAPI. Representative images are shown. ER-mitochondria co-localization is shown in gray. Scale bar = 20 μ m

H. ^3H -cholesterol was complexed with methyl- β -cyclodextrin and its incorporation and esterification in PS-DKO cells was monitored. BLT1 and U18666A were used to inhibit SR-B1 and NPC-1/Aster, respectively.

Fig. S6.

A, B. (A) Filipin staining of MFN2-WT cells incubated in either 5% FBS without added lipoproteins (\emptyset) or in serum-free medium with the different lipoproteins (HDL, LDL, VLDL) for 5 h. MFN2-KO cells with 5% FBS are also shown. Scale bar = 10 μm . **(B)** Quantification of filipin intensity present at the cytosol or around the plasma membrane, corrected by the area of the region.

C. Analysis of the effect of inhibitors of neutral or acidic SMases (GW4869 and desipramine, respectively) on cells exposed to 10% FBS or the indicated lipoproteins for 5 h. Cells were preincubated for 15 min with GW4869 or desipramine, and then treated with sphingomyelin-C16-Cy5 for the last 3h of the incubation with FBS or lipoproteins. The generation of phosphocholine-Cy5 (the SM cleavage product) is shown.

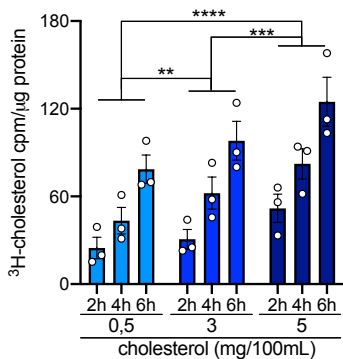
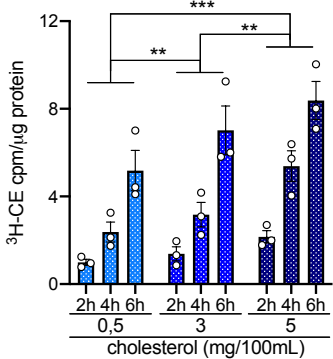
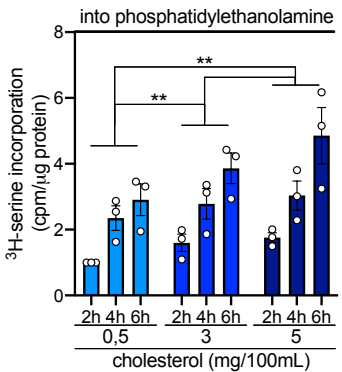
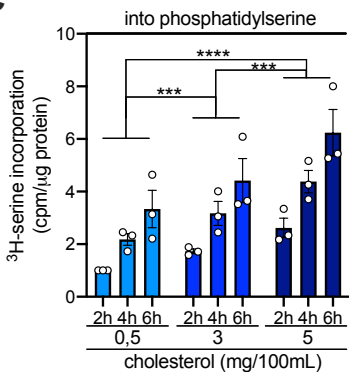
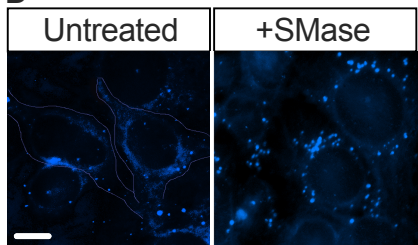
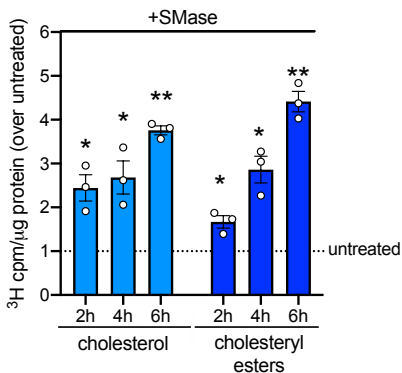
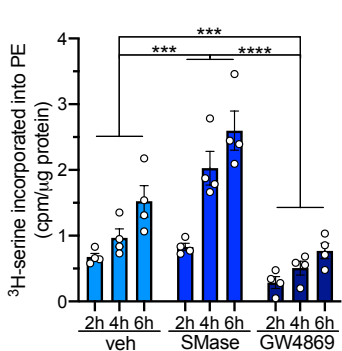
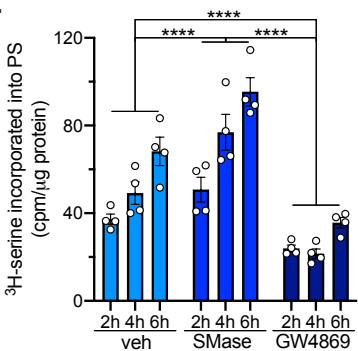
A**B****C****D****E****F**

FIGURE 1

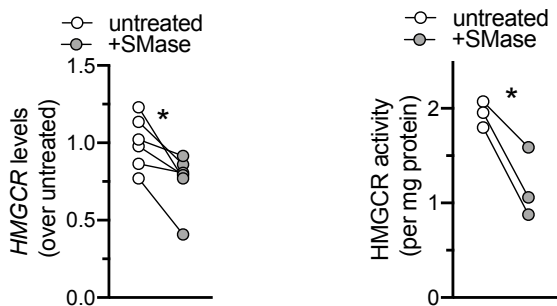
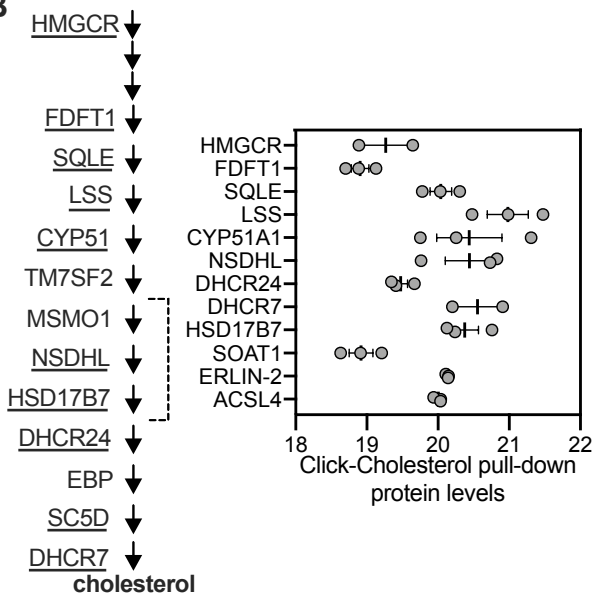
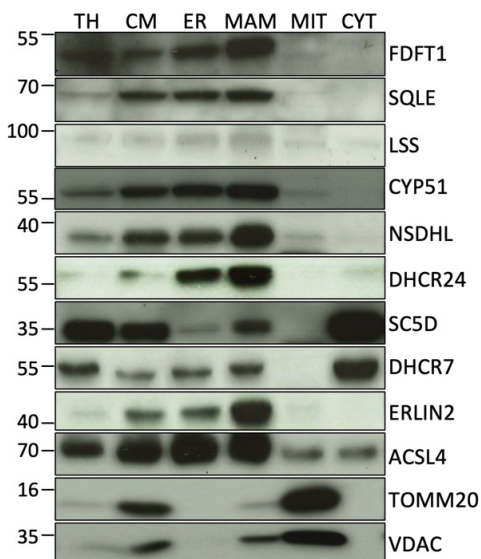
A**B****C**

FIGURE 2

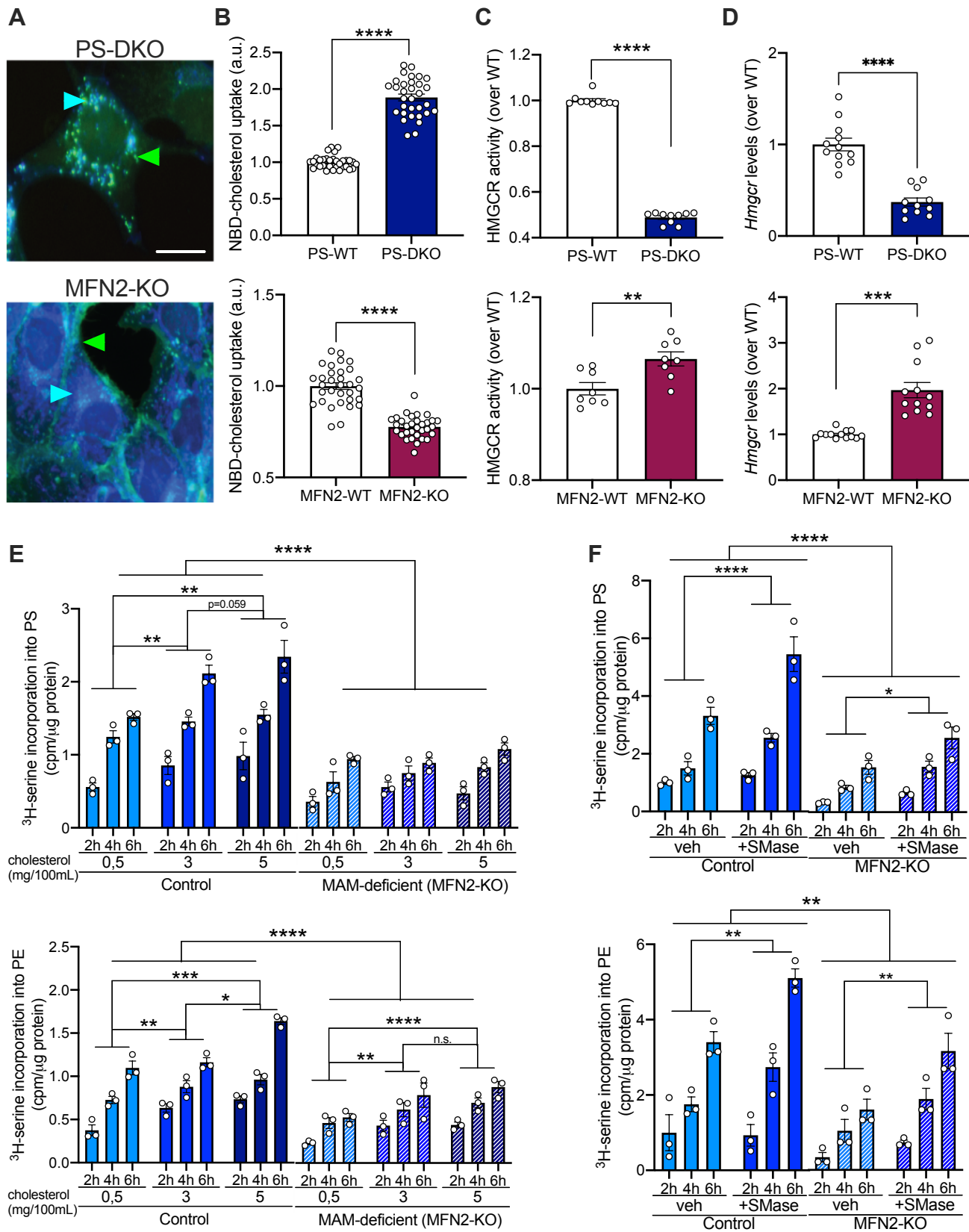


FIGURE 3

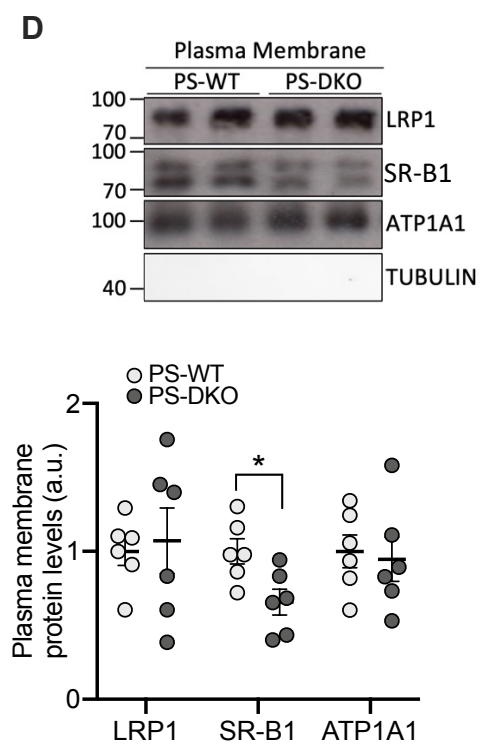
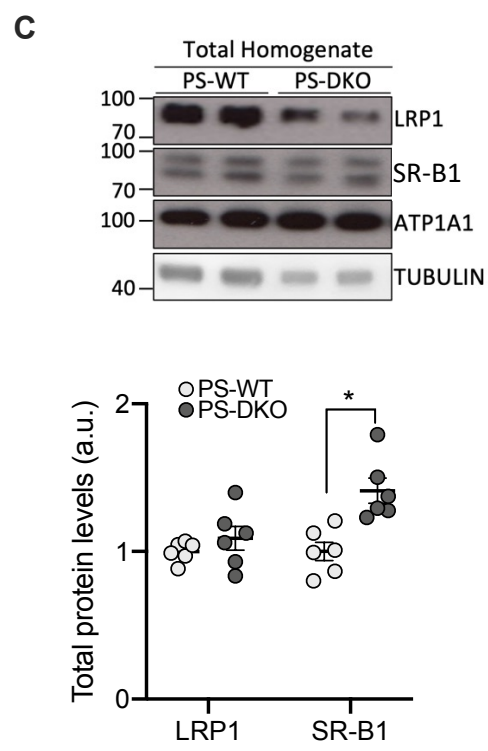
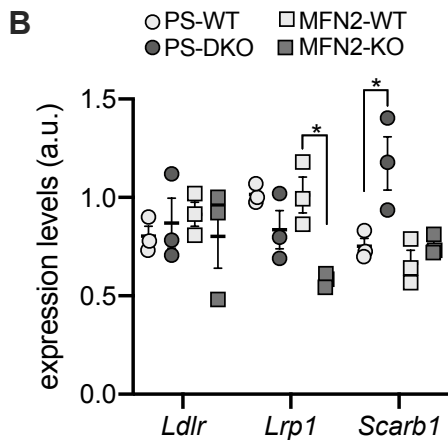
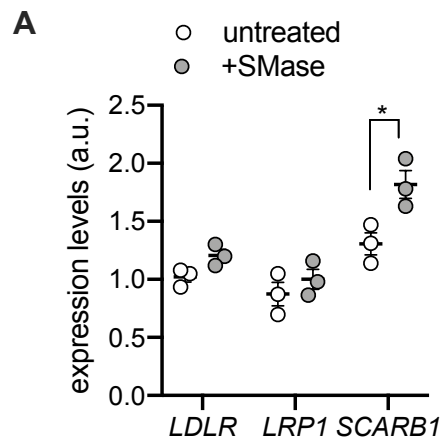


FIGURE 4

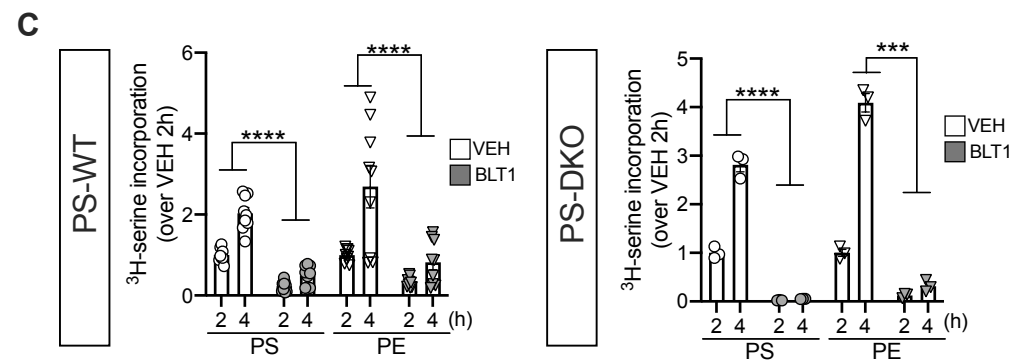
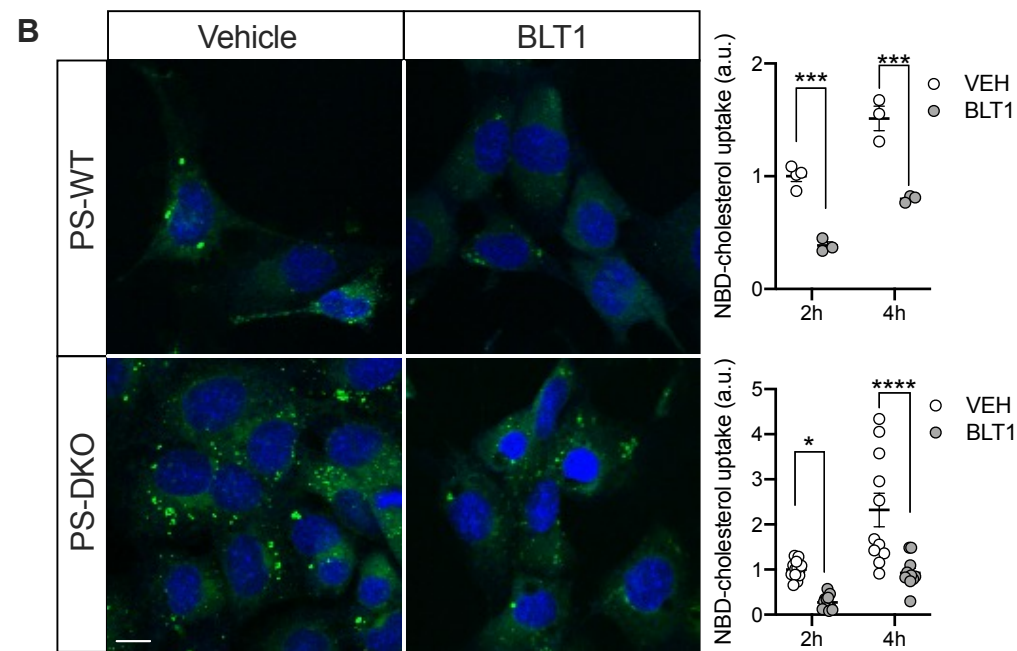
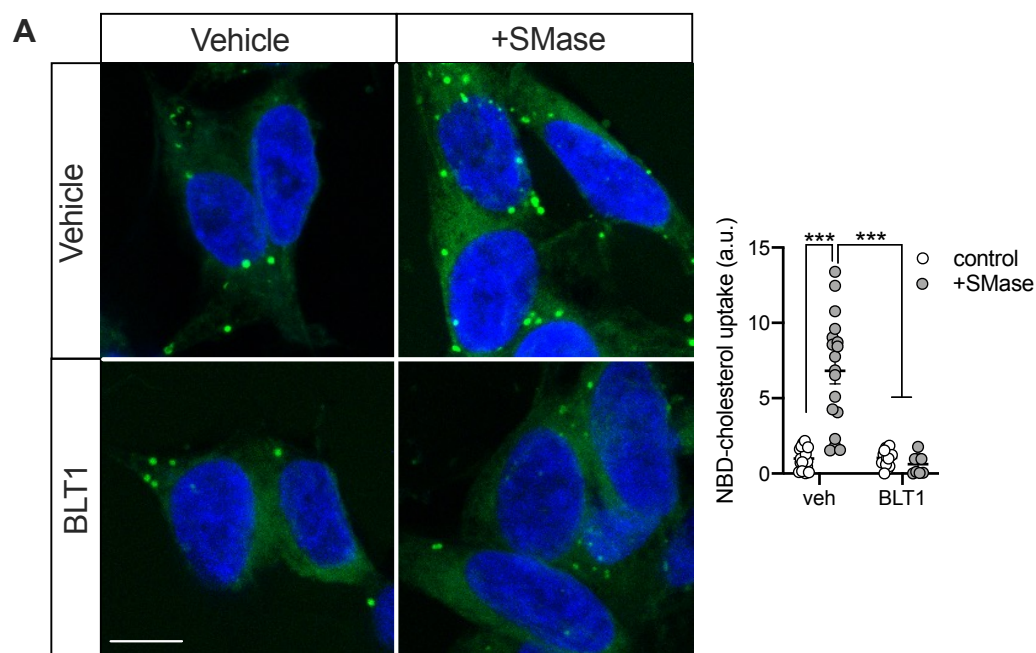


FIGURE 5

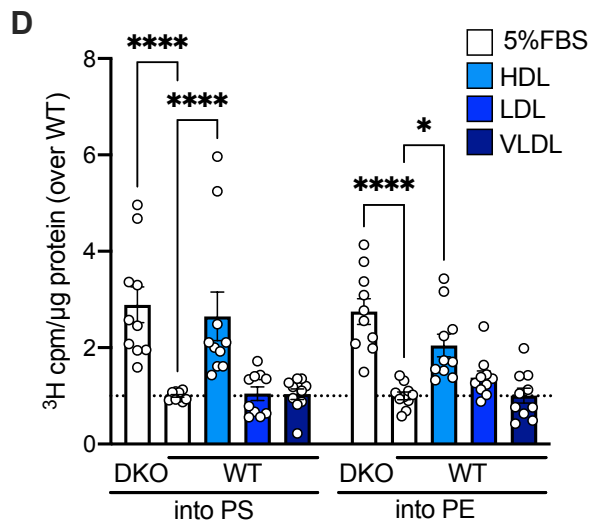
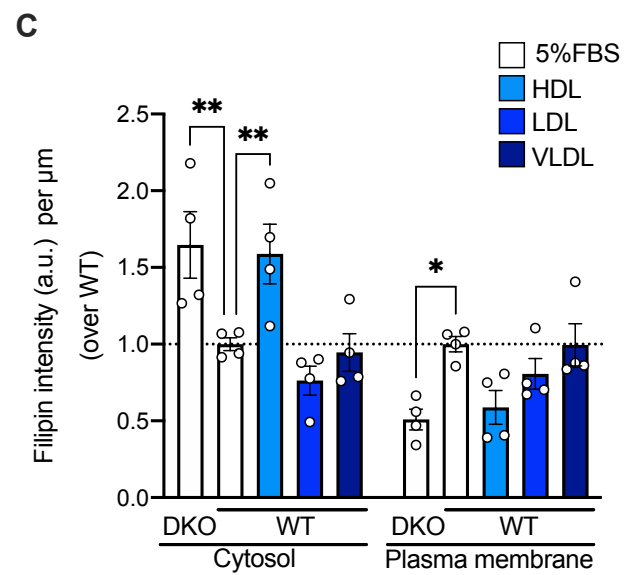
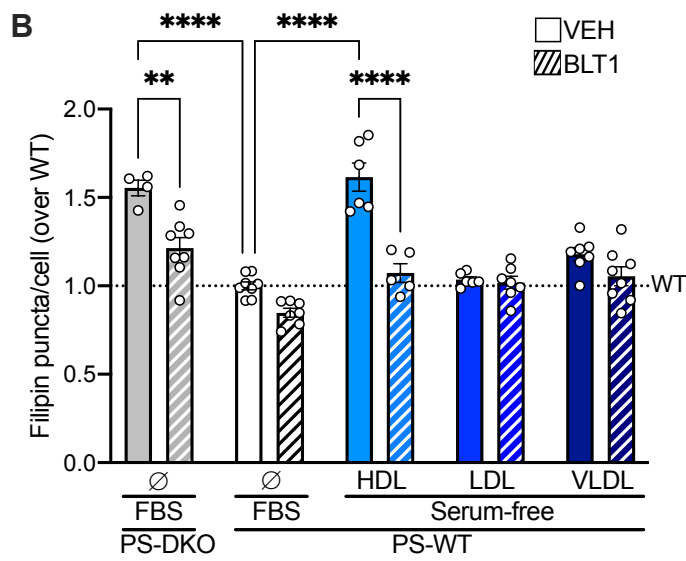
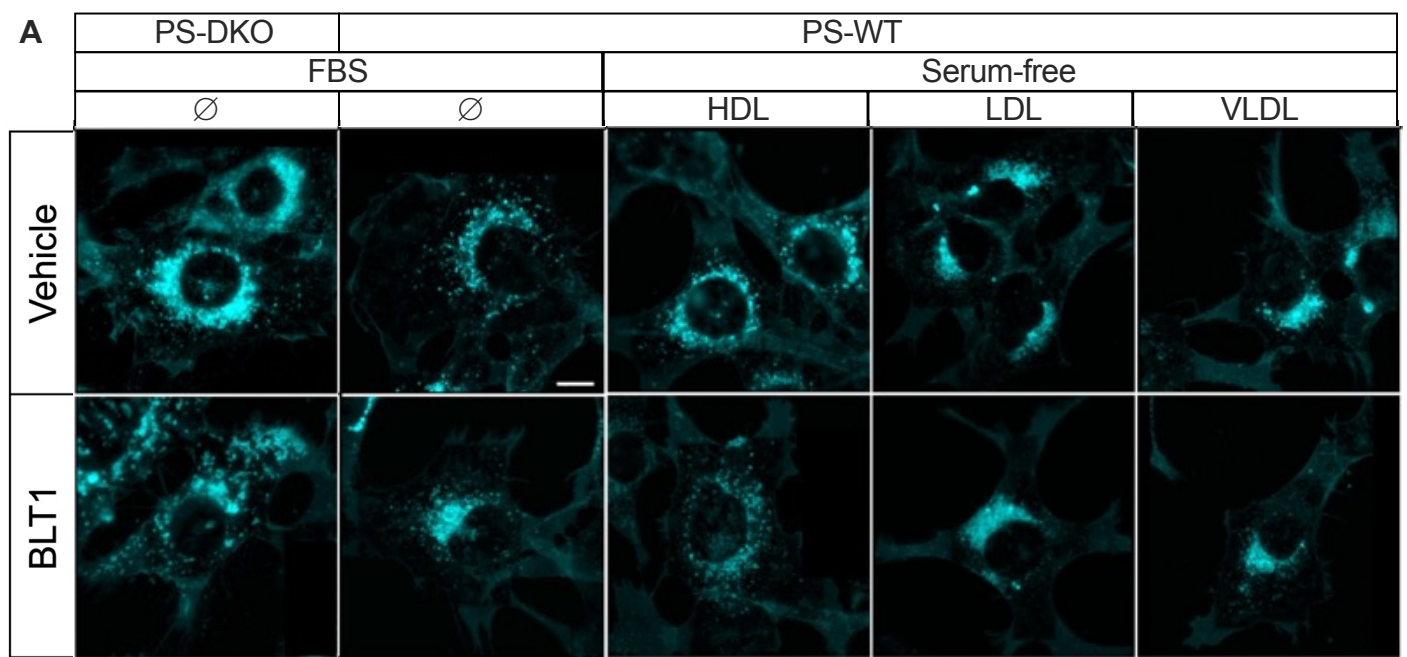
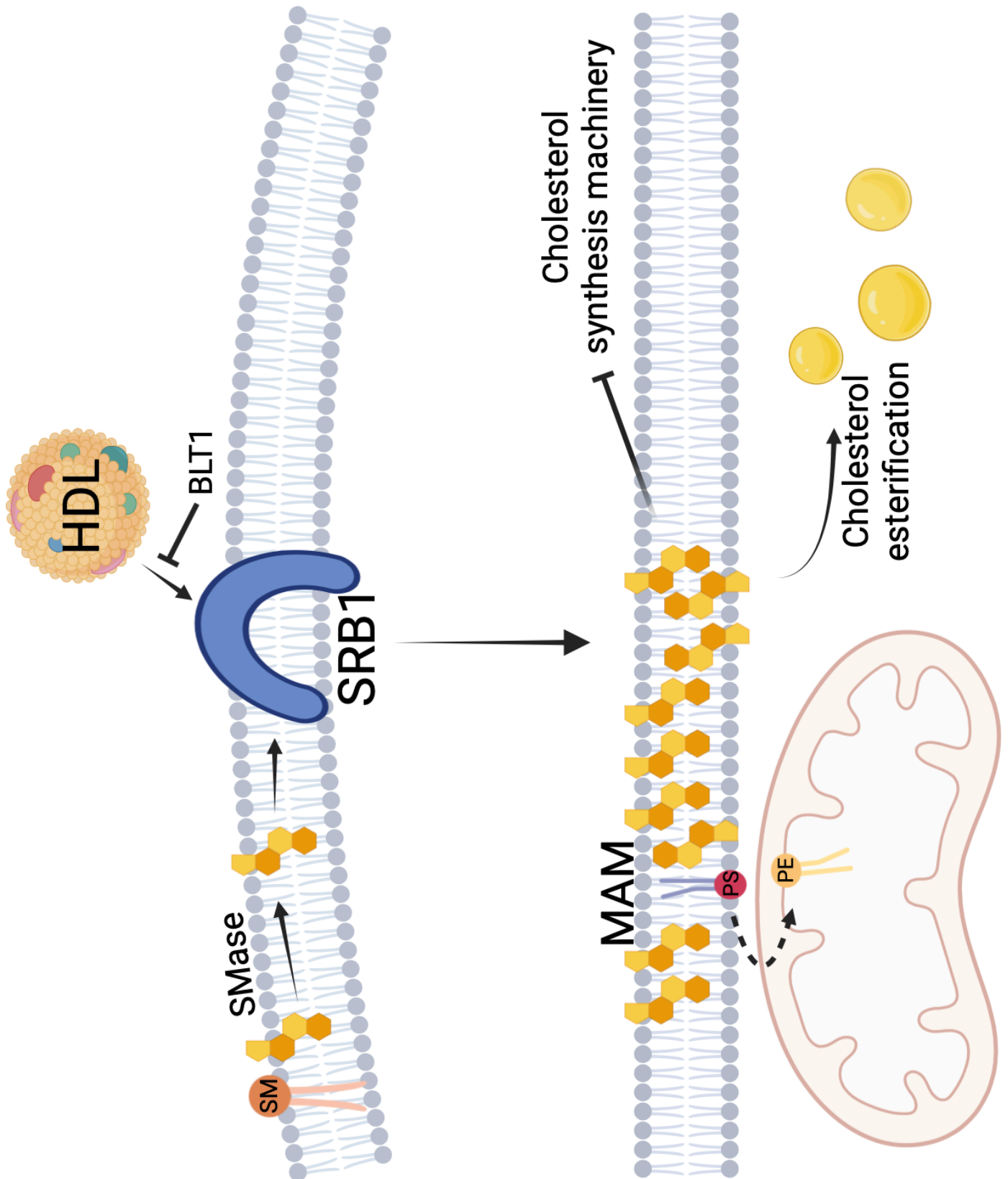


FIGURE 6



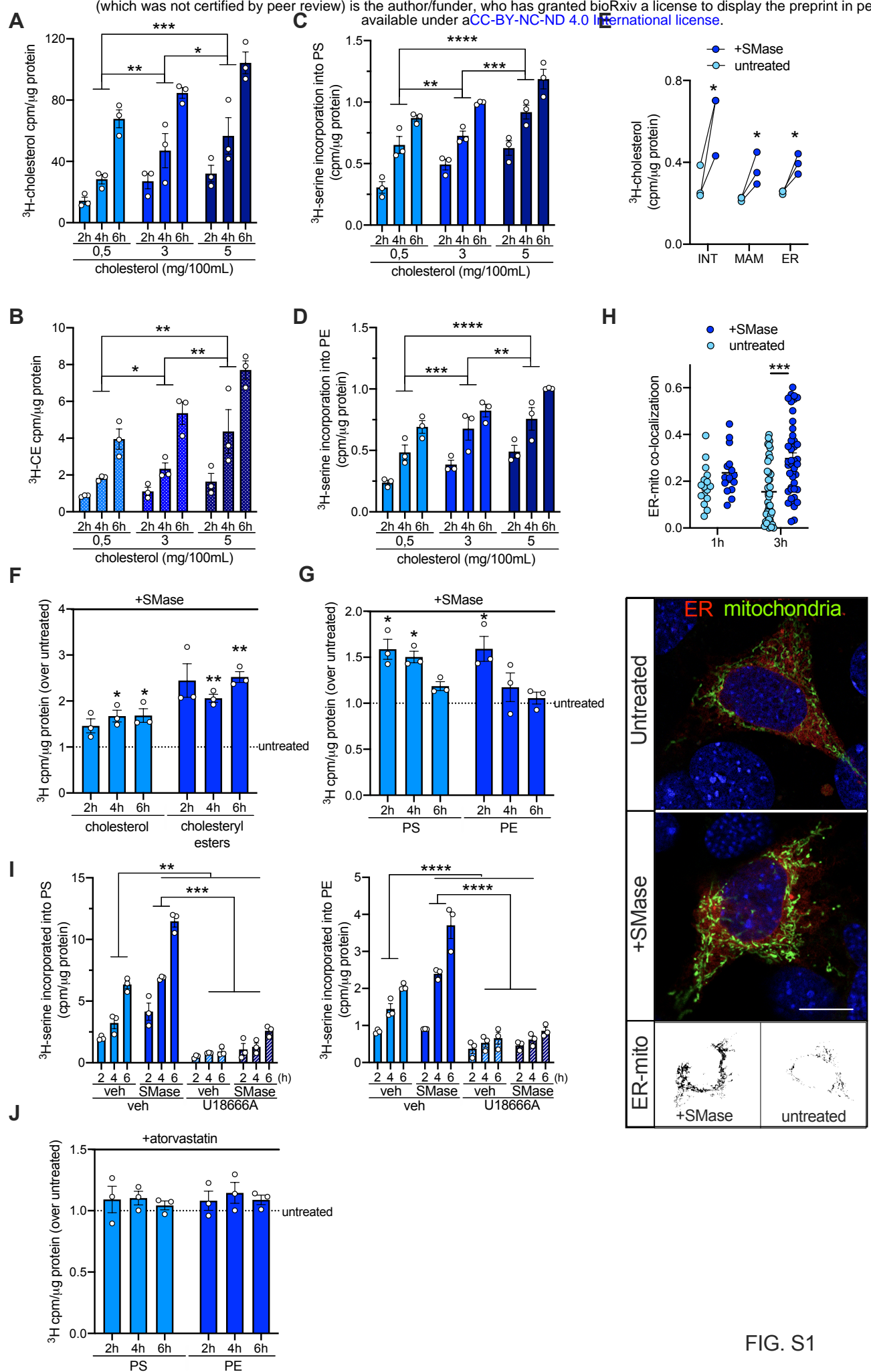


FIG. S1

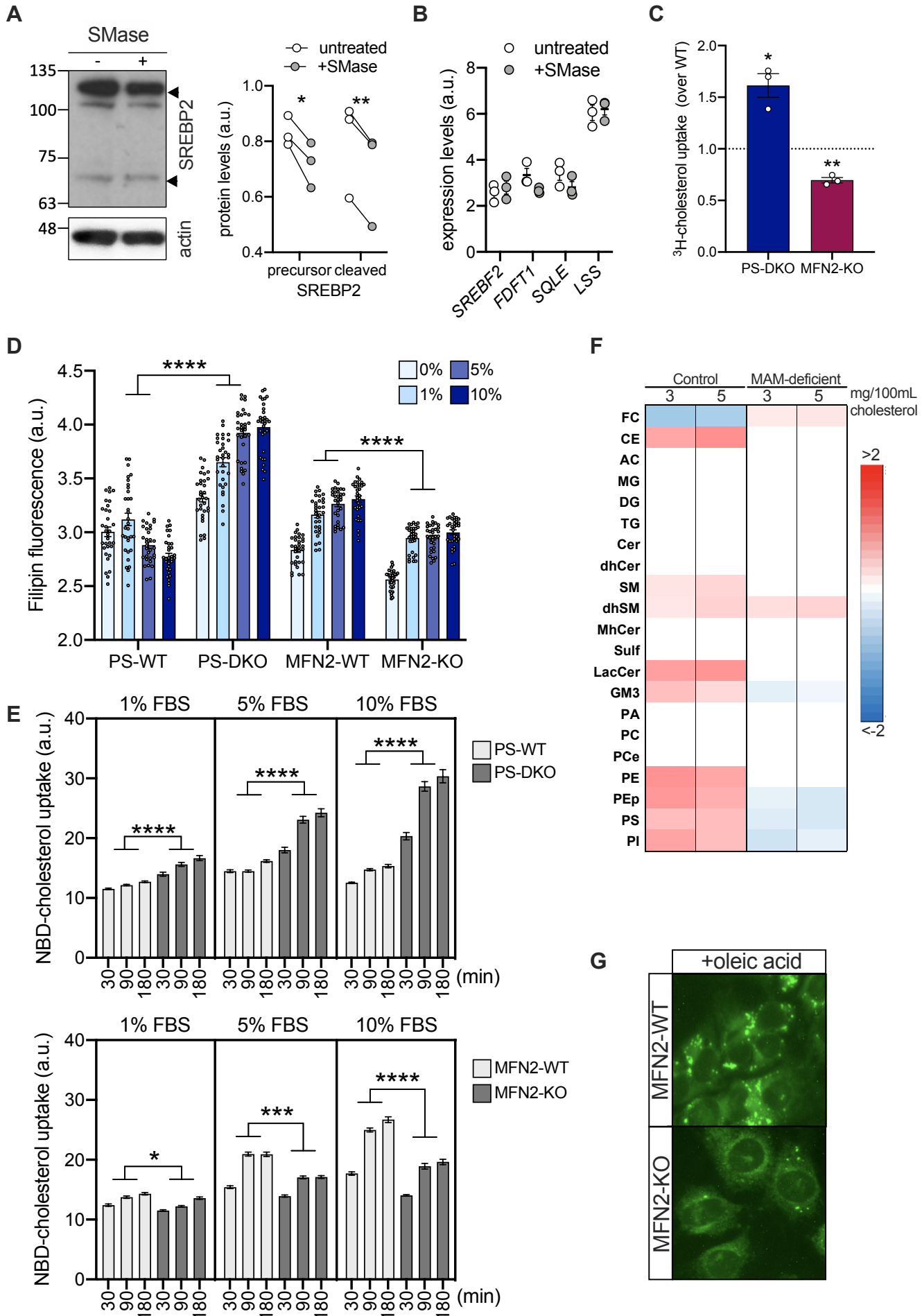


FIG. S2

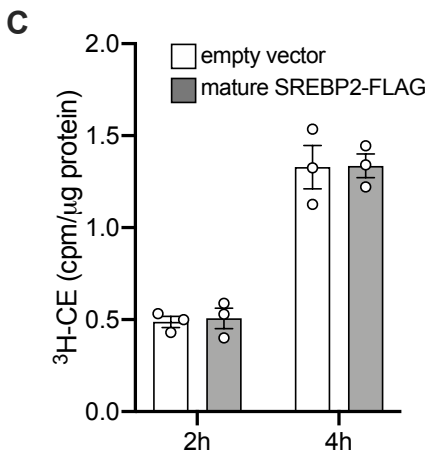
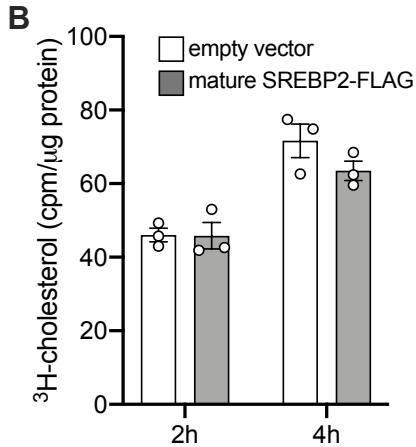
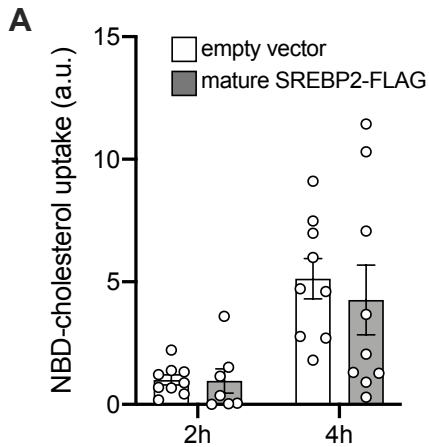
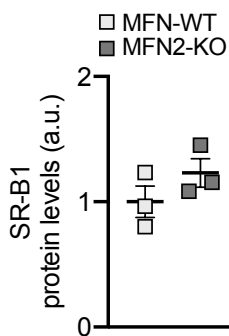
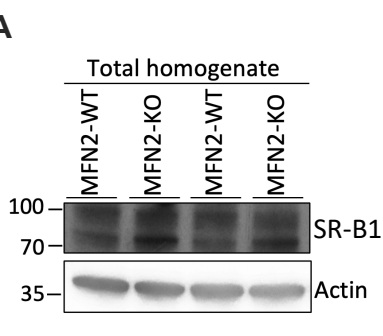
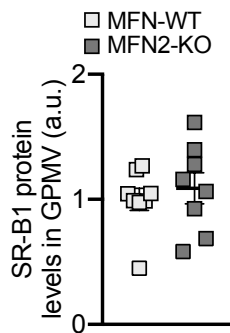
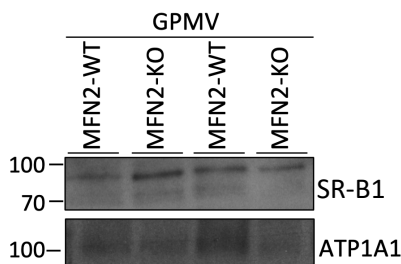
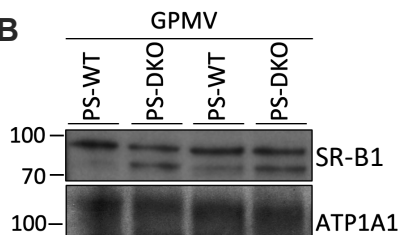


FIG. S3

A**B**

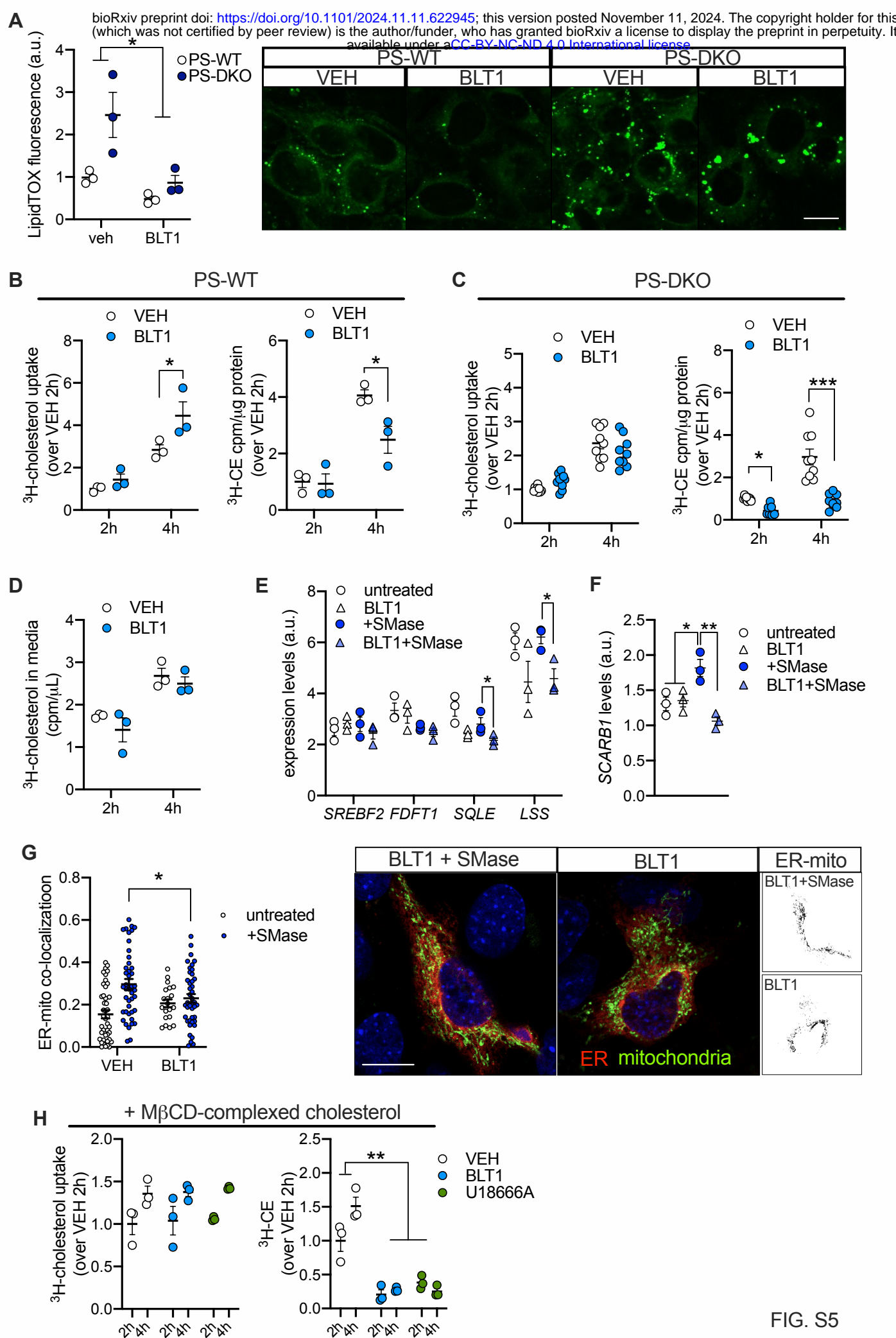


FIG. S5

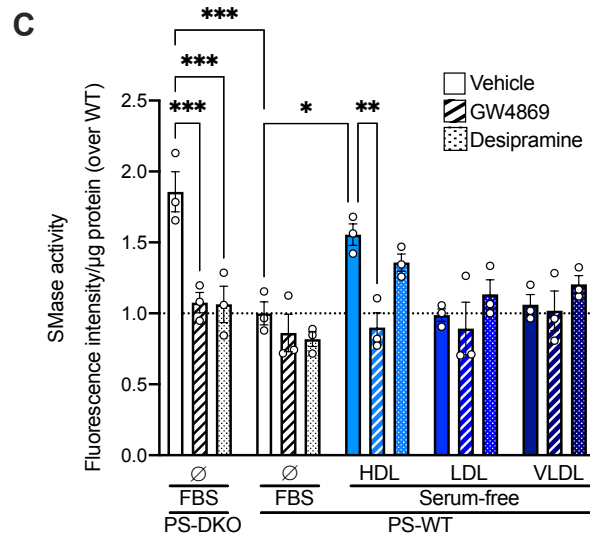
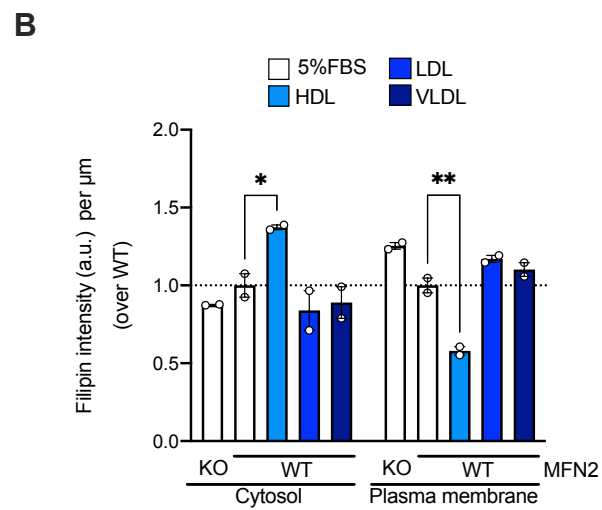
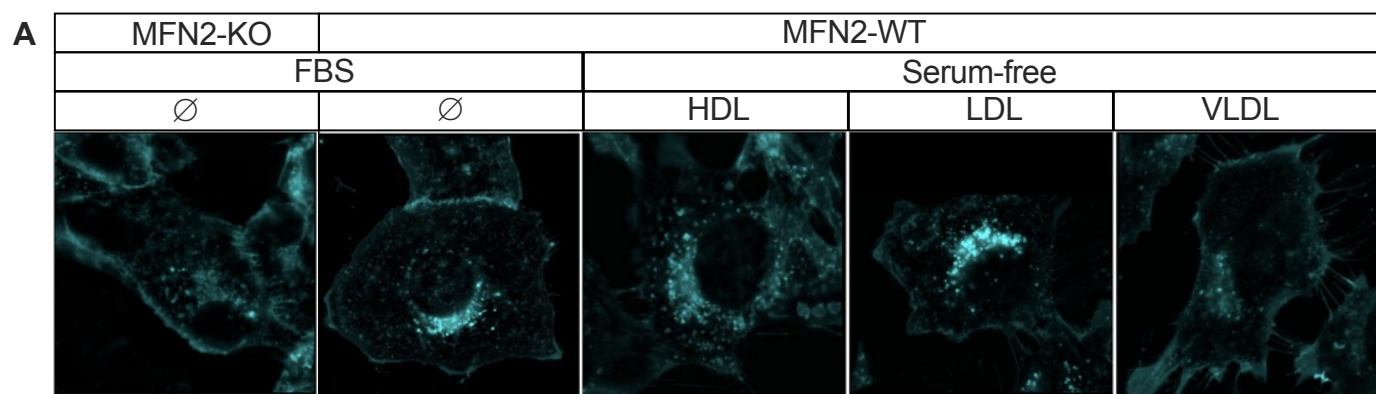


FIG. S6